



## Lingering radioactivity at the Bikini and Enewetak Atolls

Ken O. Buesseler\*, Matthew A. Charette, Steven M. Pike, Paul B. Henderson, Lauren E. Kipp

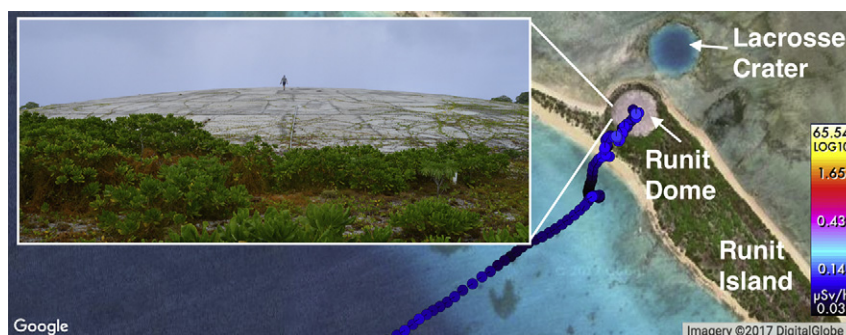
Department of Marine Chemistry and Geochemistry, Woods Hole Oceanographic Institution, Woods Hole, MA 02543, USA



### HIGHLIGHTS

- Both  $^{239,240}\text{Pu}$  and  $^{137}\text{Cs}$  remain elevated today at Bikini and Enewetak Atolls.
- These sites remain a small long term source of Pu and Cs to the North Pacific.
- About half of the Pu in the waters at Enewetak Lagoon originates near Runit Dome.
- Only a small fraction of Pu and Cs from Runit Dome is delivered via groundwater.

### GRAPHICAL ABSTRACT



### ARTICLE INFO

#### Article history:

Received 4 August 2017  
Received in revised form 5 October 2017  
Accepted 12 October 2017  
Available online 30 October 2017

Editor: D. Barcelo

#### Keywords:

Marshall Islands  
Runit dome  
Plutonium  
Cesium  
Radium  
Nuclear weapons tests

### ABSTRACT

We made an assessment of the levels of radionuclides in the ocean waters, seafloor and groundwater at Bikini and Enewetak Atolls where the US conducted nuclear weapons tests in the 1940's and 50's. This included the first estimates of submarine groundwater discharge (SGD) derived from radium isotopes that can be used here to calculate radionuclide fluxes in to the lagoon waters. While there is significant variability between sites and sample types, levels of plutonium ( $^{239,240}\text{Pu}$ ) remain several orders of magnitude higher in lagoon seawater and sediments than what is found in rest of the world's oceans. In contrast, levels of cesium-137 ( $^{137}\text{Cs}$ ) while relatively elevated in brackish groundwater are only slightly higher in the lagoon water relative to North Pacific surface waters. Of special interest was the Runit dome, a nuclear waste repository created in the 1970's within the Enewetak Atoll. Low seawater ratios of  $^{240}\text{Pu}/^{239}\text{Pu}$  suggest that this area is the source of about half of the Pu in the Enewetak lagoon water column, yet radium isotopes suggest that SGD from below the dome is not a significant Pu source. SGD fluxes of Pu and Cs at Bikini were also relatively low. Thus radioactivity associated with seafloor sediments remains the largest source and long term repository for radioactive contamination. Overall, Bikini and Enewetak Atolls are an ongoing source of Pu and Cs to the North Pacific, but at annual rates that are orders of magnitude smaller than delivered via close-in fallout to the same area.

© 2017 The Authors. Published by Elsevier B.V. This is an open access article under the CC BY license (<http://creativecommons.org/licenses/by/4.0/>).

### 1. Introduction

The US conducted 66 nuclear weapons tests at the Bikini and Enewetak Atolls between 1946 and 1958 accounting for >50% of the global fallout during that time period and 20% of global fallout by the

time atmospheric testing ended (based upon yields; Buesseler, 1997; Hamilton, 2004). Unlike most of the global fallout that was distributed widely from high altitude testing, the majority of tests were conducted either on the surface of the atoll lagoons, on the islands, or underwater. This resulted in “close-in” fallout that contaminated not only the local islands and lagoon sediments, but also larger areas of the North Pacific Ocean where close-in fallout accounts for 60% of the total fallout Pu (Bowen et al., 1980).

\* Corresponding author.  
E-mail address: [kbuesseler@whoi.edu](mailto:kbuesseler@whoi.edu) (K.O. Buesseler).

The fate of radionuclides at these islands was evaluated starting with the first atomic tests, but became more extensive after testing ended in the 1960s and again in the 1970s in preparation for resettlement of the islands (see review by Robison and Noshkin, 1999). Activities greater than background fallout levels were found for many radionuclides in lagoon waters due to their continued remobilization, presumably from marine sediments. This issue persists today, though estimated doses to humans from consumption of marine foods is thought to be a small source of the total radiological dose, for example < 0.1% at Enewetak Atoll (Robison and Noshkin, 1999). While monitoring of the ocean has largely ended and ground level radiation doses are at background (Bordner et al., 2016), there are still ongoing health studies of the populations that left the atoll islands and of the roughly 500 remaining inhabitants that have returned to live on Enewetak Island (<https://marshallislands.lnl.gov/>).

During a January 2015 expedition to the Bikini and Enewetak Atolls, we sought to determine if there have been significant changes in radionuclide levels in the water column, sediments, and groundwater. Of special interest was a possible ongoing source associated with a waste disposal site commonly known as the Runit Dome in Enewetak Atoll, where close to 100,000 cubic meters of radioactive debris were buried in a 100 m diameter nuclear testing crater in the late 1970s and covered with a concrete cap (Davison et al., 2012; Hamilton, 2013; Noshkin and Robison, 1997). The debris was a combination of contaminated Enewetak soils, coral materials, scrap metal, excess equipment and some Pu-bearing nuclear material that was explosively scattered over the island of Runit during a test in 1958 (Quince) and other debris from low-yield tests in the Runit Island area.

Plutonium isotope ratios from individual tests are known to vary based upon the nuclear weapons design and fission and fusion yields, with higher yields resulting in the production of higher mass Pu isotopes. The Quince test did not result in any nuclear yield or fission, but deposited weapons grade Pu in the lagoon sediments near Runit Island, some of which was buried under the dome with a distinct and lower  $^{240}\text{Pu}/^{239}\text{Pu}$  atom ratio than from other tests. Other sites of interest included Bravo Crater in Bikini Atoll and Mike Crater in Enewetak Atoll, where the largest US thermonuclear (hydrogen bomb) tests were conducted. These two high yield tests resulted in the largest deposition of close-in fallout, and high  $^{240}\text{Pu}/^{239}\text{Pu}$  ratios that are characteristic of the North Pacific today relative to other ocean regions that received only global fallout (Buesseler, 1997; Diamond et al., 1960; Kelley et al., 1999).

In this study we sampled seawater, groundwater and lagoon sediments at selected sites with an emphasis on Pu isotopes ( $^{239}\text{Pu}$   $t_{1/2} = 24,100$  yr.;  $^{240}\text{Pu}$   $t_{1/2} = 6560$  yr.) and radiocesium ( $^{137}\text{Cs}$   $t_{1/2} = 30.1$  yr.). These artificial radionuclides have been widely studied in the ocean with Pu's distribution being influenced by its tendency to be scavenged by particles as well as mixed with ocean currents, whereas Cs is predominantly a more conservative water mass tracer (e.g. Livingston and Povinec, 2000). In addition to Pu and Cs, sediments were examined for two other gamma emitters- americium-241 ( $^{241}\text{Am}$ ) and bismuth-207 ( $^{207}\text{Bi}$ ), both of which would be relatively particle-reactive in the ocean. Americium-241 is the decay product of  $^{241}\text{Pu}$  ( $t_{1/2} = 14.3$  yr.), which is produced during the blasts in variable amounts and thus similar to  $^{239}\text{Pu}$  and  $^{240}\text{Pu}$ , preferentially found associated with the sites of the highest yield tests.  $^{207}\text{Bi}$  was readily detectable in only one core collected during this study and likely generated by an unusual fusion device test that resulted in its production via activation of stable bismuth, or deuterium capture in lead; hence it is not readily detectable in global fallout (Aarkrog et al., 1984; Noshkin et al., 2001).

In addition to the artificial radionuclides, the naturally occurring isotopes of radium ( $^{224}\text{Ra}$ ,  $^{223}\text{Ra}$ ,  $^{228}\text{Ra}$ ,  $^{226}\text{Ra}$ ) were measured in parallel with the artificial radionuclides in order to quantify their input to the lagoons from submarine groundwater discharge (Burnett et al., 2006; Charette et al., 2008). They were measured in wells on land and groundwater underlying the beaches to look at the flux of groundwater

between the islands and the lagoons, including between the Runit Dome and Enewetak Lagoon. To our knowledge, these are the first direct estimates of groundwater-surface water exchange rates for artificial radionuclides at the site of the Marshall Islands US nuclear weapons testing program. Water column ratios of short- to long-lived Ra isotopes provide an estimate of the lagoon flushing times (Charette et al., 2013), useful for calculating artificial radionuclide fluxes from the lagoons to the Pacific Ocean.

Our primary goal was to make an independent reassessment in 2015 of the levels of the major fallout radionuclides that remain in the lagoon waters and seafloor of Bikini and Enewetak Atolls, some 60–70 years after nuclear testing ended. We accomplished this by comparing our data within the lagoons to values measured earlier at these sites and as found elsewhere globally. The levels of radionuclides from these nuclear tests are also compared to the world's largest accidental release of radionuclides to the ocean in 2011 associated with the Fukushima Dai-ichi nuclear power plants. A secondary goal was to address for the first time the relative importance of Pu contamination to the Enewetak lagoon that originates from the Runit Dome area, either via submarine groundwater discharge or from surrounding lagoon sediments.

## 2. Sampling and methods

### 2.1. Physical setting

The Bikini and Enewetak Atolls are among the 29 atolls that make up the Republic of the Marshall Islands, located in the equatorial Pacific some 4000 km west of Hawaii. Geographically, the Bikini Atoll is centered at 11° 35' N 165° 23' E and consists of 26 islands (23 remaining after weapons testing) with an area of 8.8 km<sup>2</sup> that form a roughly circular reef that surrounds a lagoon of 630 km<sup>2</sup> area with a mean depth of 46 m. Enewetak is centered on 11° 30' N 162° 15' E with a ring of 42 islands (39 remaining) of 6.9 km<sup>2</sup> area and a lagoon of 932 km<sup>2</sup> area and mean depth of 48 m. The collective land area of the 1000's of small islands that make up the Marshall Islands is only equivalent to the area of Washington DC (180 km<sup>2</sup>), yet they are spread across an ocean area that exceeds the size of Alaska (1,900,000 km<sup>2</sup>). Both atolls are low lying with an average elevation of 2–3 m, thus in addition to the radiological concern, sea level rise will have immediate consequences for these atolls.

These two remote atolls were selected for US nuclear testing and became known as the western part of the US Pacific Proving Grounds (PPG). Given the different designs of the nuclear devices and range of yields, there is in effect a mosaic of different radionuclides and contamination levels associated with particular test sites within the lagoons. Also, given that there were commonly several tests at the same site, for example, 7 within the Bravo Crater (Noshkin et al., 2001) and 17 close to or on Runit Island (Noshkin and Robison, 1997), local contamination cannot often be ascribed to a single test as there is intermingled fallout debris from multiple blasts throughout these atolls.

### 2.2. Sampling

The primary sampling in this study took place in and around the Bikini Atoll from January 18 to 20, followed by the Enewetak Atoll from January 22 to 24, 2015, with one sampling site mid-way between the atolls and one surface seawater sample collected outside of the entrance to each lagoon (Fig. 1). The sampling was conducted aboard the *M/V Alucia*, a 185 ft (56 m) vessel provided by the Dalio Foundation and operated for scientific sampling in partnership with the Woods Hole Oceanographic Institution. A seawater profile in the Pacific collected just prior to our cruise between Guam and Majuro, Marshall Islands was collected to represent the open (Pacific) ocean end-member for radionuclide activities and isotope ratios.

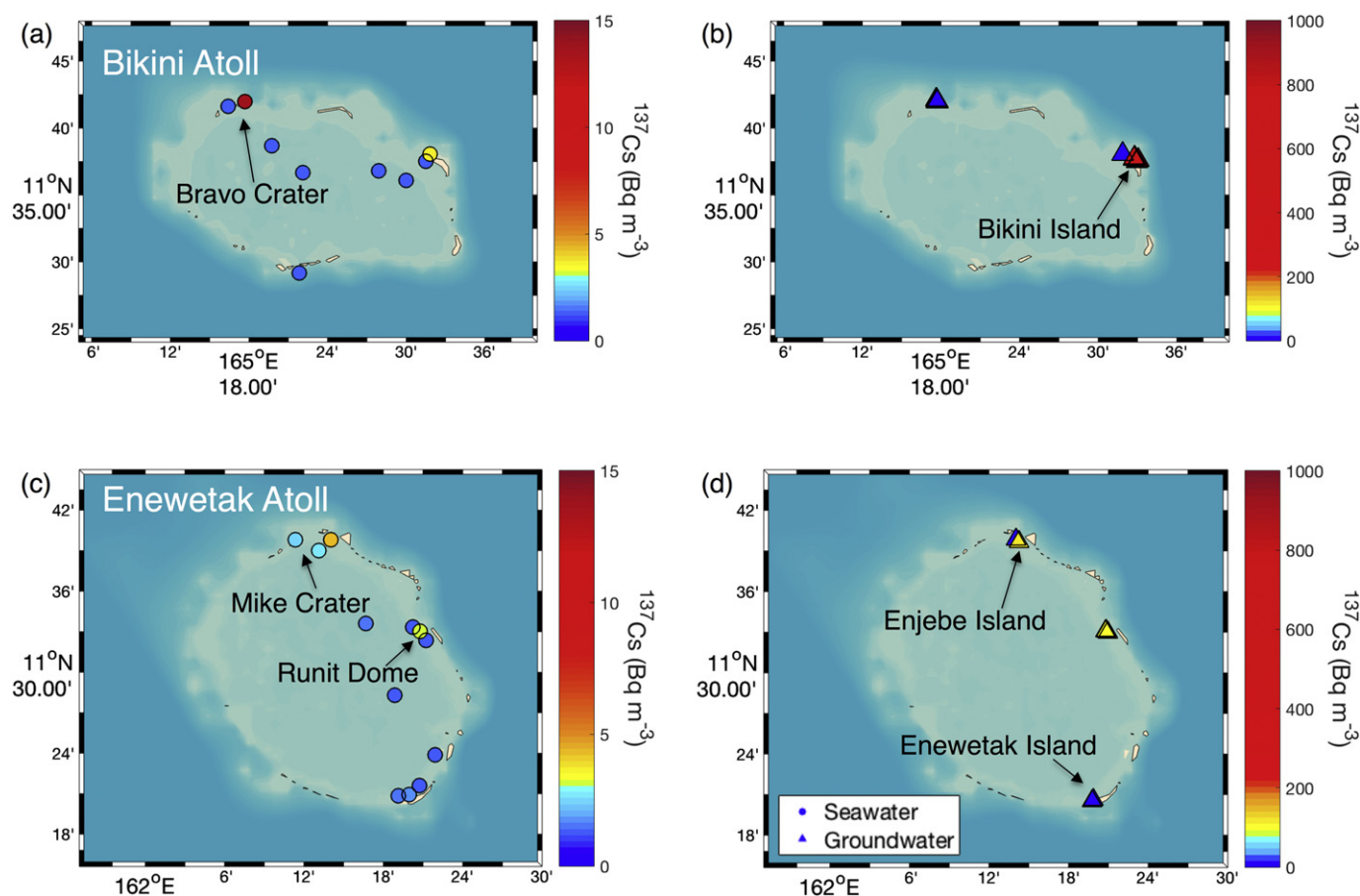


**Fig. 1.** Activities of  $^{137}\text{Cs}$  in seawater (circles) and groundwater (triangles) from Bikini (a, b) and Enewetak (c, d) atolls for both surface seawater and groundwater samples. Scales are colour coded in  $\text{Bq m}^{-3}$  as indicated.

### 2.2.1. Seawater

Surface seawater samples were collected using a metal free large volume pump with a three place manifold for simultaneous sampling. Barrels for radium processing were filled with 400–600 L, during which time samples for Cs, Pu and salinity were collected. Barrel samples for short and long-lived radium isotopes were filtered through  $\text{MnO}_2$ -impregnated acrylic fibers at  $<0.5 \text{ L min}^{-1}$  to quantitatively adsorb Ra (Moore and Reid, 1973). Pu samples were taken from a separate port on the pump manifold using acid clean sampling lines and acid clean 2 to 4 L bottles. The same pump system was used to fill 10–20 L plastic cubitainers for surface Cs, as well as manually filling of the cubitainers in some locations. A standard CTD/Rosette was used for collecting depth resolved water column profiles in the Bravo and Mike craters and at a site outside of the Marshall Islands. Pu and Cs samples from the CTD were collected using the same methods as the barrel samples. It should be noted that seawater collected in this study via surface pump or CTD was unfiltered.

### 2.2.2. Groundwater

We collected groundwater samples from previously installed monitoring wells, cement cisterns and piezometers installed in various locations along the beaches. A peristaltic pump was attached to push point piezometers (MHE products) by way of acid cleaned Tygon tubing and connected to a flow through cell to measure basic water properties using an YSI sonde. The YSI was precalibrated with Ricca pH and conductivity standards. Oxygen was calibrated using the YSI in air method as described in the manual. Extra samples were collected at each site to confirm YSI salinity measurements and analyzed by a Guideline salinometer. Groundwater from PVC wells and cisterns was collected

in a similar way, replacing the peristaltic pump with a plastic well pump with a low flow controller (Proactive Cyclone/MiniMonsoon). In all cases, the wells and piezometers were purged by extracting  $3 \times$  the casing volume prior to sample collection. Water sampled for short- and long-lived radium isotopes was pumped into 20 L cubitainers and gravity filtered at  $<0.5 \text{ L min}^{-1}$  to quantitatively adsorb Ra onto  $\text{MnO}_2$ -impregnated acrylic fibers (Moore and Reid, 1973). Plutonium and cesium samples were collected as detailed above.

### 2.2.3. Seafloor sediments

Sediment cores were collected at four sites: Bravo and Mike craters, and near Bikini and Runit Islands. Cores were manually extracted by divers using 6 cm diameter acrylic push tubes and ranged in depth from 16 to 80 cm. In the lab, cores were sectioned at 2 cm intervals and dried at  $50^\circ\text{C}$  until a constant weight was achieved. Dried sections were ground, sub sampled and weighed into acrylic counting vials for analysis by gamma spectroscopy.

## 2.3. Analyses

### 2.3.1. Cesium extraction from water samples

Cesium extraction from seawater and groundwater samples was performed at sea on 10–20 L samples. A stable  $^{133}\text{Cs}$  carrier (0.6–0.95 mg/ml standard) was added to each sample, shaken and allowed to equilibrate before an initial aliquot of 1 ml was collected for stable cesium recovery corrections (Pike et al., 2013). Using a peristaltic pump, samples were filtered through 5 ml of KNiFC-PAN resin (Sebesta, 1997) at a flow rate of 45–55 ml per minute. After passing through the column, the processed samples were collected into clean cubitainers and a final 1 ml aliquot was taken for recovery analysis. The KNiFC-PAN

was then transferred to a 30 ml acrylic vial for gamma analysis (Breier et al., 2016). Results for Cs are in good agreement with seawater reference material SRM IAEA-443 (Pike et al., 2013).

### 2.3.2. Sediment and water gamma spectrometry

Gamma counting of all sediment samples was performed using two High Purity Germanium (HPGe) well detectors. The SAGe Well MN# GSW275L (Canberra) is a closed-ended germanium coaxial detector with a well 28 mm in diameter, 40 mm depth and active crystal volume of 275 cm<sup>3</sup>. The second traditional HPGe Well MN# GCW4030S (Canberra) detector is also a closed-ended germanium detector with a well diameter of 28 mm, depth of 45 mm and active crystal volume of 190 cm<sup>3</sup>. Both detectors were equipped with cosmic-veto suppression systems with signal processing through Lynx MCA (Canberra) digital signal analyzers. Data was acquired through Prospect and Genie 2000 software (Canberra). Both detectors have an energy range from 10 to 1500 keV and detection limit of 0.001 cps. Isotopes and energies measured in sediments were <sup>241</sup>Am at 59.5 keV, <sup>207</sup>Pb at 248 keV, <sup>214</sup>Pb at 242 keV, <sup>214</sup>Pb at 295 keV, <sup>214</sup>Pb at 352 keV, <sup>214</sup>Pb at 409 keV, <sup>214</sup>Pb at 464 keV, <sup>214</sup>Pb at 511 keV, <sup>214</sup>Pb at 569 keV, <sup>214</sup>Pb at 609 keV, <sup>214</sup>Pb at 661 keV, <sup>214</sup>Pb at 720 keV, <sup>214</sup>Pb at 784 keV, <sup>214</sup>Pb at 846 keV, <sup>214</sup>Pb at 911 keV, <sup>214</sup>Pb at 979 keV, <sup>214</sup>Pb at 1044 keV, <sup>214</sup>Pb at 1112 keV, <sup>214</sup>Pb at 1180 keV, <sup>214</sup>Pb at 1248 keV, <sup>214</sup>Pb at 1316 keV, <sup>214</sup>Pb at 1384 keV, <sup>214</sup>Pb at 1452 keV, <sup>214</sup>Pb at 1519 keV, <sup>214</sup>Pb at 1587 keV, <sup>214</sup>Pb at 1655 keV, <sup>214</sup>Pb at 1723 keV, <sup>214</sup>Pb at 1791 keV, <sup>214</sup>Pb at 1859 keV, <sup>214</sup>Pb at 1927 keV, <sup>214</sup>Pb at 1995 keV, <sup>214</sup>Pb at 2063 keV, <sup>214</sup>Pb at 2131 keV, <sup>214</sup>Pb at 2199 keV, <sup>214</sup>Pb at 2267 keV, <sup>214</sup>Pb at 2335 keV, <sup>214</sup>Pb at 2403 keV, <sup>214</sup>Pb at 2471 keV, <sup>214</sup>Pb at 2539 keV, <sup>214</sup>Pb at 2607 keV, <sup>214</sup>Pb at 2675 keV, <sup>214</sup>Pb at 2743 keV, <sup>214</sup>Pb at 2811 keV, <sup>214</sup>Pb at 2879 keV, <sup>214</sup>Pb at 2947 keV, <sup>214</sup>Pb at 3015 keV, <sup>214</sup>Pb at 3083 keV, <sup>214</sup>Pb at 3151 keV, <sup>214</sup>Pb at 3219 keV, <sup>214</sup>Pb at 3287 keV, <sup>214</sup>Pb at 3355 keV, <sup>214</sup>Pb at 3423 keV, <sup>214</sup>Pb at 3491 keV, <sup>214</sup>Pb at 3559 keV, <sup>214</sup>Pb at 3627 keV, <sup>214</sup>Pb at 3695 keV, <sup>214</sup>Pb at 3763 keV, <sup>214</sup>Pb at 3831 keV, <sup>214</sup>Pb at 3899 keV, <sup>214</sup>Pb at 3967 keV, <sup>214</sup>Pb at 4035 keV, <sup>214</sup>Pb at 4103 keV, <sup>214</sup>Pb at 4171 keV, <sup>214</sup>Pb at 4239 keV, <sup>214</sup>Pb at 4307 keV, <sup>214</sup>Pb at 4375 keV, <sup>214</sup>Pb at 4443 keV, <sup>214</sup>Pb at 4511 keV, <sup>214</sup>Pb at 4579 keV, <sup>214</sup>Pb at 4647 keV, <sup>214</sup>Pb at 4715 keV, <sup>214</sup>Pb at 4783 keV, <sup>214</sup>Pb at 4851 keV, <sup>214</sup>Pb at 4919 keV, <sup>214</sup>Pb at 4987 keV, <sup>214</sup>Pb at 5055 keV, <sup>214</sup>Pb at 5123 keV, <sup>214</sup>Pb at 5191 keV, <sup>214</sup>Pb at 5259 keV, <sup>214</sup>Pb at 5327 keV, <sup>214</sup>Pb at 5395 keV, <sup>214</sup>Pb at 5463 keV, <sup>214</sup>Pb at 5531 keV, <sup>214</sup>Pb at 5599 keV, <sup>214</sup>Pb at 5667 keV, <sup>214</sup>Pb at 5735 keV, <sup>214</sup>Pb at 5803 keV, <sup>214</sup>Pb at 5871 keV, <sup>214</sup>Pb at 5939 keV, <sup>214</sup>Pb at 6007 keV, <sup>214</sup>Pb at 6075 keV, <sup>214</sup>Pb at 6143 keV, <sup>214</sup>Pb at 6211 keV, <sup>214</sup>Pb at 6279 keV, <sup>214</sup>Pb at 6347 keV, <sup>214</sup>Pb at 6415 keV, <sup>214</sup>Pb at 6483 keV, <sup>214</sup>Pb at 6551 keV, <sup>214</sup>Pb at 6619 keV, <sup>214</sup>Pb at 6687 keV, <sup>214</sup>Pb at 6755 keV, <sup>214</sup>Pb at 6823 keV, <sup>214</sup>Pb at 6891 keV, <sup>214</sup>Pb at 6959 keV, <sup>214</sup>Pb at 7027 keV, <sup>214</sup>Pb at 7095 keV, <sup>214</sup>Pb at 7163 keV, <sup>214</sup>Pb at 7231 keV, <sup>214</sup>Pb at 7299 keV, <sup>214</sup>Pb at 7367 keV, <sup>214</sup>Pb at 7435 keV, <sup>214</sup>Pb at 7503 keV, <sup>214</sup>Pb at 7571 keV, <sup>214</sup>Pb at 7639 keV, <sup>214</sup>Pb at 7707 keV, <sup>214</sup>Pb at 7775 keV, <sup>214</sup>Pb at 7843 keV, <sup>214</sup>Pb at 7911 keV, <sup>214</sup>Pb at 7979 keV, <sup>214</sup>Pb at 8047 keV, <sup>214</sup>Pb at 8115 keV, <sup>214</sup>Pb at 8183 keV, <sup>214</sup>Pb at 8251 keV, <sup>214</sup>Pb at 8319 keV, <sup>214</sup>Pb at 8387 keV, <sup>214</sup>Pb at 8455 keV, <sup>214</sup>Pb at 8523 keV, <sup>214</sup>Pb at 8591 keV, <sup>214</sup>Pb at 8659 keV, <sup>214</sup>Pb at 8727 keV, <sup>214</sup>Pb at 8795 keV, <sup>214</sup>Pb at 8863 keV, <sup>214</sup>Pb at 8931 keV, <sup>214</sup>Pb at 8999 keV, <sup>214</sup>Pb at 9067 keV, <sup>214</sup>Pb at 9135 keV, <sup>214</sup>Pb at 9203 keV, <sup>214</sup>Pb at 9271 keV, <sup>214</sup>Pb at 9339 keV, <sup>214</sup>Pb at 9407 keV, <sup>214</sup>Pb at 9475 keV, <sup>214</sup>Pb at 9543 keV, <sup>214</sup>Pb at 9611 keV, <sup>214</sup>Pb at 9679 keV, <sup>214</sup>Pb at 9747 keV, <sup>214</sup>Pb at 9815 keV, <sup>214</sup>Pb at 9883 keV, <sup>214</sup>Pb at 9951 keV, <sup>214</sup>Pb at 10019 keV, <sup>214</sup>Pb at 10087 keV, <sup>214</sup>Pb at 10155 keV, <sup>214</sup>Pb at 10223 keV, <sup>214</sup>Pb at 10291 keV, <sup>214</sup>Pb at 10359 keV, <sup>214</sup>Pb at 10427 keV, <sup>214</sup>Pb at 10495 keV, <sup>214</sup>Pb at 10563 keV, <sup>214</sup>Pb at 10631 keV, <sup>214</sup>Pb at 10699 keV, <sup>214</sup>Pb at 10767 keV, <sup>214</sup>Pb at 10835 keV, <sup>214</sup>Pb at 10903 keV, <sup>214</sup>Pb at 10971 keV, <sup>214</sup>Pb at 11039 keV, <sup>214</sup>Pb at 11107 keV, <sup>214</sup>Pb at 11175 keV, <sup>214</sup>Pb at 11243 keV, <sup>214</sup>Pb at 11311 keV, <sup>214</sup>Pb at 11379 keV, <sup>214</sup>Pb at 11447 keV, <sup>214</sup>Pb at 11515 keV, <sup>214</sup>Pb at 11583 keV, <sup>214</sup>Pb at 11651 keV, <sup>214</sup>Pb at 11719 keV, <sup>214</sup>Pb at 11787 keV, <sup>214</sup>Pb at 11855 keV, <sup>214</sup>Pb at 11923 keV, <sup>214</sup>Pb at 11991 keV, <sup>214</sup>Pb at 12059 keV, <sup>214</sup>Pb at 12127 keV, <sup>214</sup>Pb at 12195 keV, <sup>214</sup>Pb at 12263 keV, <sup>214</sup>Pb at 12331 keV, <sup>214</sup>Pb at 12399 keV, <sup>214</sup>Pb at 12467 keV, <sup>214</sup>Pb at 12535 keV, <sup>214</sup>Pb at 12603 keV, <sup>214</sup>Pb at 12671 keV, <sup>214</sup>Pb at 12739 keV, <sup>214</sup>Pb at 12807 keV, <sup>214</sup>Pb at 12875 keV, <sup>214</sup>Pb at 12943 keV, <sup>214</sup>Pb at 13011 keV, <sup>214</sup>Pb at 13079 keV, <sup>214</sup>Pb at 13147 keV, <sup>214</sup>Pb at 13215 keV, <sup>214</sup>Pb at 13283 keV, <sup>214</sup>Pb at 13351 keV, <sup>214</sup>Pb at 13419 keV, <sup>214</sup>Pb at 13487 keV, <sup>214</sup>Pb at 13555 keV, <sup>214</sup>Pb at 13623 keV, <sup>214</sup>Pb at 13691 keV, <sup>214</sup>Pb at 13759 keV, <sup>214</sup>Pb at 13827 keV, <sup>214</sup>Pb at 13895 keV, <sup>214</sup>Pb at 13963 keV, <sup>214</sup>Pb at 14031 keV, <sup>214</sup>Pb at 14099 keV, <sup>214</sup>Pb at 14167 keV, <sup>214</sup>Pb at 14235 keV, <sup>214</sup>Pb at 14303 keV, <sup>214</sup>Pb at 14371 keV, <sup>214</sup>Pb at 14439 keV, <sup>214</sup>Pb at 14507 keV, <sup>214</sup>Pb at 14575 keV, <sup>214</sup>Pb at 14643 keV, <sup>214</sup>Pb at 14711 keV, <sup>214</sup>Pb at 14779 keV, <sup>214</sup>Pb at 14847 keV, <sup>214</sup>Pb at 14915 keV, <sup>214</sup>Pb at 14983 keV, <sup>214</sup>Pb at 15051 keV, <sup>214</sup>Pb at 15119 keV, <sup>214</sup>Pb at 15187 keV, <sup>214</sup>Pb at 15255 keV, <sup>214</sup>Pb at 15323 keV, <sup>214</sup>Pb at 15391 keV, <sup>214</sup>Pb at 15459 keV, <sup>214</sup>Pb at 15527 keV, <sup>214</sup>Pb at 15595 keV, <sup>214</sup>Pb at 15663 keV, <sup>214</sup>Pb at 15731 keV, <sup>214</sup>Pb at 15799 keV, <sup>214</sup>Pb at 15867 keV, <sup>214</sup>Pb at 15935 keV, <sup>214</sup>Pb at 16003 keV, <sup>214</sup>Pb at 16071 keV, <sup>214</sup>Pb at 16139 keV, <sup>214</sup>Pb at 16207 keV, <sup>214</sup>Pb at 16275 keV, <sup>214</sup>Pb at 16343 keV, <sup>214</sup>Pb at 16411 keV, <sup>214</sup>Pb at 16479 keV, <sup>214</sup>Pb at 16547 keV, <sup>214</sup>Pb at 16615 keV, <sup>214</sup>Pb at 16683 keV, <sup>214</sup>Pb at 16751 keV, <sup>214</sup>Pb at 16819 keV, <sup>214</sup>Pb at 16887 keV, <sup>214</sup>Pb at 16955 keV, <sup>214</sup>Pb at 17023 keV, <sup>214</sup>Pb at 17091 keV, <sup>214</sup>Pb at 17159 keV, <sup>214</sup>Pb at 17227 keV, <sup>214</sup>Pb at 17295 keV, <sup>214</sup>Pb at 17363 keV, <sup>214</sup>Pb at 17431 keV, <sup>214</sup>Pb at 17499 keV, <sup>214</sup>Pb at 17567 keV, <sup>214</sup>Pb at 17635 keV, <sup>214</sup>Pb at 17703 keV, <sup>214</sup>Pb at 17771 keV, <sup>214</sup>Pb at 17839 keV, <sup>214</sup>Pb at 17907 keV, <sup>214</sup>Pb at 17975 keV, <sup>214</sup>Pb at 18043 keV, <sup>214</sup>Pb at 18111 keV, <sup>214</sup>Pb at 18179 keV, <sup>214</sup>Pb at 18247 keV, <sup>214</sup>Pb at 18315 keV, <sup>214</sup>Pb at 18383 keV, <sup>214</sup>Pb at 18451 keV, <sup>214</sup>Pb at 18519 keV, <sup>214</sup>Pb at 18587 keV, <sup>214</sup>Pb at 18655 keV, <sup>214</sup>Pb at 18723 keV, <sup>214</sup>Pb at 18791 keV, <sup>214</sup>Pb at 18859 keV, <sup>214</sup>Pb at 18927 keV, <sup>214</sup>Pb at 18995 keV, <sup>214</sup>Pb at 19063 keV, <sup>214</sup>Pb at 19131 keV, <sup>214</sup>Pb at 19199 keV, <sup>214</sup>Pb at 19267 keV, <sup>214</sup>Pb at 19335 keV, <sup>214</sup>Pb at 19403 keV, <sup>214</sup>Pb at 19471 keV, <sup>214</sup>Pb at 19539 keV, <sup>214</sup>Pb at 19607 keV, <sup>214</sup>Pb at 19675 keV, <sup>214</sup>Pb at 19743 keV, <sup>214</sup>Pb at 19811 keV, <sup>214</sup>Pb at 19879 keV, <sup>214</sup>Pb at 19947 keV, <sup>214</sup>Pb at 20015 keV, <sup>214</sup>Pb at 20083 keV, <sup>214</sup>Pb at 20151 keV, <sup>214</sup>Pb at 20219 keV, <sup>214</sup>Pb at 20287 keV, <sup>214</sup>Pb at 20355 keV, <sup>214</sup>Pb at 20423 keV, <sup>214</sup>Pb at 20491 keV, <sup>214</sup>Pb at 20559 keV, <sup>214</sup>Pb at 20627 keV, <sup>214</sup>Pb at 20695 keV, <sup>214</sup>Pb at 20763 keV, <sup>214</sup>Pb at 20831 keV, <sup>214</sup>Pb at 20899 keV, <sup>214</sup>Pb at 20967 keV, <sup>214</sup>Pb at 21035 keV, <sup>214</sup>Pb at 21103 keV, <sup>214</sup>Pb at 21171 keV, <sup>214</sup>Pb at 21239 keV, <sup>214</sup>Pb at 21307 keV, <sup>214</sup>Pb at 21375 keV, <sup>214</sup>Pb at 21443 keV, <sup>214</sup>Pb at 21511 keV, <sup>214</sup>Pb at 21579 keV, <sup>214</sup>Pb at 21647 keV, <sup>214</sup>Pb at 21715 keV, <sup>214</sup>Pb at 21783 keV, <sup>214</sup>Pb at 21851 keV, <sup>214</sup>Pb at 21919 keV, <sup>214</sup>Pb at 21987 keV, <sup>214</sup>Pb at 22055 keV, <sup>214</sup>Pb at 22123 keV, <sup>214</sup>Pb at 22191 keV, <sup>214</sup>Pb at 22259 keV, <sup>214</sup>Pb at 22327 keV, <sup>214</sup>Pb at 22395 keV, <sup>214</sup>Pb at 22463 keV, <sup>214</sup>Pb at 22531 keV, <sup>214</sup>Pb at 22599 keV, <sup>214</sup>Pb at 22667 keV, <sup>214</sup>Pb at 22735 keV, <sup>214</sup>Pb at 22803 keV, <sup>214</sup>Pb at 22871 keV, <sup>214</sup>Pb at 22939 keV, <sup>214</sup>Pb at 23007 keV, <sup>214</sup>Pb at 23075 keV, <sup>214</sup>Pb at 23143 keV, <sup>214</sup>Pb at 23211 keV, <sup>214</sup>Pb at 23279 keV, <sup>214</sup>Pb at 23347 keV, <sup>214</sup>Pb at 23415 keV, <sup>214</sup>Pb at 23483 keV, <sup>214</sup>Pb at 23551 keV, <sup>214</sup>Pb at 23619 keV, <sup>214</sup>Pb at 23687 keV, <sup>214</sup>Pb at 23755 keV, <sup>214</sup>Pb at 23823 keV, <sup>214</sup>Pb at 23891 keV, <sup>214</sup>Pb at 23959 keV, <sup>214</sup>Pb at 24027 keV, <sup>214</sup>Pb at 24095 keV, <sup>214</sup>Pb at 24163 keV, <sup>214</sup>Pb at 24231 keV, <sup>214</sup>Pb at 24299 keV, <sup>214</sup>Pb at 24367 keV, <sup>214</sup>Pb at 24435 keV, <sup>214</sup>Pb at 24503 keV, <sup>214</sup>Pb at 24571 keV, <sup>214</sup>Pb at 24639 keV, <sup>214</sup>Pb at 24707 keV, <sup>214</sup>Pb at 24775 keV, <sup>214</sup>Pb at 24843 keV, <sup>214</sup>Pb at 24911 keV, <sup>214</sup>Pb at 24979 keV, <sup>214</sup>Pb at 25047 keV, <sup>214</sup>Pb at 25115 keV, <sup>214</sup>Pb at 25183 keV, <sup>214</sup>Pb at 25251 keV, <sup>214</sup>Pb at 25319 keV, <sup>214</sup>Pb at 25387 keV, <sup>214</sup>Pb at 25455 keV, <sup>214</sup>Pb at 25523 keV, <sup>214</sup>Pb at 25591 keV, <sup>214</sup>Pb at 25659 keV, <sup>214</sup>Pb at 25727 keV, <sup>214</sup>Pb at 25795 keV, <sup>214</sup>Pb at 25863 keV, <sup>214</sup>Pb at 25931 keV, <sup>214</sup>Pb at 26000 keV, <sup>214</sup>Pb at 26068 keV, <sup>214</sup>Pb at 26136 keV, <sup>214</sup>Pb at 26204 keV, <sup>214</sup>Pb at 26272 keV, <sup>214</sup>Pb at 26340 keV, <sup>214</sup>Pb at 26408 keV, <sup>214</sup>Pb at 26476 keV, <sup>214</sup>Pb at 26544 keV, <sup>214</sup>Pb at 26612 keV, <sup>214</sup>Pb at 26680 keV, <sup>214</sup>Pb at 26748 keV, <sup>214</sup>Pb at 26816 keV, <sup>214</sup>Pb at 26884 keV, <sup>214</sup>Pb at 26952 keV, <sup>214</sup>Pb at 27020 keV, <sup>214</sup>Pb at 27088 keV, <sup>214</sup>Pb at 27156 keV, <sup>214</sup>Pb at 27224 keV, <sup>214</sup>Pb at 27292 keV, <sup>214</sup>Pb at 27360 keV, <sup>214</sup>Pb at 27428 keV, <sup>214</sup>Pb at 27496 keV, <sup>214</sup>Pb at 27564 keV, <sup>214</sup>Pb at 27632 keV, <sup>214</sup>Pb at 27700 keV, <sup>214</sup>Pb at 27768 keV, <sup>214</sup>Pb at 27836 keV, <sup>214</sup>Pb at 27904 keV, <sup>214</sup>Pb at 27972 keV, <sup>214</sup>Pb at 28040 keV, <sup>214</sup>Pb at 28108 keV, <sup>214</sup>Pb at 28176 keV, <sup>214</sup>Pb at 28244 keV, <sup>214</sup>Pb at 28312 keV, <sup>214</sup>Pb at 28380 keV, <sup>214</sup>Pb at 28448 keV, <sup>214</sup>Pb at 28516 keV, <sup>214</sup>Pb at 28584 keV, <sup>214</sup>Pb at 28652 keV, <sup>214</sup>Pb at 28720 keV, <sup>214</sup>Pb at 28788 keV, <sup>214</sup>Pb at 28856 keV, <sup>214</sup>Pb at 28924 keV, <sup>214</sup>Pb at 28992 keV, <sup>214</sup>Pb at 29060 keV, <sup>214</sup>Pb at 29128 keV, <sup>214</sup>Pb at 29196 keV, <sup>214</sup>Pb at 29264 keV, <sup>214</sup>Pb at 29332 keV, <sup>214</sup>Pb at 29400 keV, <sup>214</sup>Pb at 29468 keV, <sup>214</sup>Pb at 29536 keV, <sup>214</sup>Pb at 29604 keV, <sup>214</sup>Pb at 29672 keV, <sup>214</sup>Pb at 29740 keV, <sup>214</sup>Pb at 29808 keV, <sup>214</sup>Pb at 29876 keV, <sup>214</sup>Pb at 29944 keV, <sup>214</sup>Pb at 30012 keV, <sup>214</sup>Pb at 30080 keV, <sup>214</sup>Pb at 30148 keV, <sup>214</sup>Pb at 30216 keV, <sup>214</sup>Pb at 30284 keV, <sup>214</sup>Pb at 30352 keV, <sup>214</sup>Pb at 30420 keV, <sup>214</sup>Pb at 30488 keV, <sup>214</sup>Pb at 30556 keV, <sup>214</sup>Pb at 30624 keV, <sup>214</sup>Pb at 30692 keV, <sup>214</sup>Pb at 30760 keV, <sup>214</sup>Pb at 30828 keV, <sup>214</sup>Pb at 30896 keV, <sup>214</sup>Pb at 30964 keV, <sup>214</sup>Pb at 31032 keV, <sup>214</sup>Pb at 31100 keV, <sup>214</sup>Pb at 31168 keV, <sup>214</sup>Pb at 31236 keV, <sup>214</sup>Pb at 31304 keV, <sup>214</sup>Pb at 31372 keV, <sup>214</sup>Pb at 31440 keV, <sup>214</sup>Pb at 31508 keV, <sup>214</sup>Pb at 31576 keV, <sup>214</sup>Pb at 31644 keV, <sup>214</sup>Pb at 31712 keV, <sup>214</sup>Pb at 31780 keV, <sup>214</sup>Pb at 31848 keV, <sup>214</sup>Pb at 31916 keV, <sup>214</sup>Pb at 31984 keV, <sup>214</sup>Pb at 32052 keV, <sup>214</sup>Pb at 32120 keV, <sup>214</sup>Pb at 32188 keV, <sup>214</sup>Pb at 32256 keV, <sup>214</sup>Pb at 32324 keV, <sup>214</sup>Pb at 32392 keV, <sup>214</sup>Pb at 32460 keV, <sup>214</sup>Pb at 32528 keV, <sup>214</sup>Pb at 32596 keV, <sup>214</sup>Pb at 32664 keV, <sup>214</sup>Pb at 32732 keV, <sup>214</sup>Pb at 32800 keV, <sup>214</sup>Pb at 32868 keV, <sup>214</sup>Pb at 32936 keV, <sup>214</sup>Pb at 33004 keV, <sup>214</sup>Pb at 33072 keV, <sup>214</sup>Pb at 33140 keV, <sup>214</sup>Pb at 33208 keV, <sup>214</sup>Pb at 33276 keV, <sup>214</sup>Pb at 33344 keV, <sup>214</sup>Pb at 33412 keV, <sup>214</sup>Pb at 33480 keV, <sup>214</sup>Pb at 33548 keV, <sup>214</sup>Pb at 33616 keV, <sup>214</sup>Pb at 33684 keV, <sup>214</sup>Pb at 33752 keV, <sup>214</sup>Pb at 33820 keV, <sup>214</sup>Pb at 33888 keV, <sup>214</sup>Pb at 33956 keV, <sup>214</sup>Pb at 34024 keV, <sup>214</sup>Pb at 34092 keV, <sup>214</sup>Pb at 34160 keV, <sup>214</sup>Pb at 34228 keV, <sup>214</sup>Pb at 34296 keV, <sup>214</sup>Pb at 34364 keV, <sup>214</sup>Pb at 34432 keV, <sup>214</sup>Pb at 34500 keV, <sup>214</sup>Pb at 34568 keV, <sup>214</sup>Pb at 34636 keV, <sup>214</sup>Pb at 34704 keV, <sup>214</sup>Pb at 34772 keV, <sup>214</sup>Pb at 34840 keV, <sup>214</sup>Pb at 34908 keV, <sup>214</sup>Pb at 34976 keV, <sup>214</sup>Pb at 35044 keV, <sup>214</sup>Pb at 35112 keV, <sup>214</sup>Pb at 35180 keV, <sup>214</sup>Pb at 35248 keV, <sup>214</sup>Pb at 35316 keV, <sup>214</sup>Pb at 35384 keV, <sup>214</sup>Pb at 35452 keV, <sup>214</sup>Pb at 35520 keV, <sup>214</sup>Pb at 35588 keV, <sup>214</sup>Pb at 35656 keV, <sup>214</sup>Pb at 35724 keV, <sup>214</sup>Pb at 35792 keV, <sup>214</sup>Pb at 35860 keV, <sup>214</sup>Pb at 35928 keV, <sup>214</sup>Pb at 36000 keV, <sup>214</sup>Pb at 36068 keV, <sup>214</sup>Pb at 36136 keV, <sup>214</sup>Pb at 36204 keV, <sup>214</sup>Pb at 36272 keV, <sup>214</sup>Pb at 36340 keV, <sup>214</sup>Pb at 36408 keV, <sup>214</sup>Pb at 36476 keV, <sup>214</sup>Pb at 36544 keV, <sup>214</sup>Pb at 36612 keV, <sup>214</sup>Pb at 36680 keV, <sup>214</sup>Pb at 36748 keV, <sup>214</sup>Pb at 36816 keV, <sup>214</sup>Pb at 36884 keV, <sup>214</sup>Pb at 36952 keV, <sup>214</sup>Pb at 37020 keV, <sup>214</sup>Pb at 37088 keV, <sup>214</sup>Pb at 37156 keV, <sup>214</sup>Pb at 37224 keV, <sup>214</sup>Pb at 37292 keV, <sup>214</sup>Pb at 37360 keV, <sup>214</sup>Pb at 37428 keV, <sup>214</sup>Pb at 37496 keV, <sup>214</sup>Pb at 37564 keV, <sup>214</sup>Pb at 37632 keV, <sup>214</sup>Pb at 37700 keV, <sup>214</sup>Pb at 37768 keV, <sup>214</sup>Pb at 37836 keV, <sup>214</sup>Pb at 37904 keV, <sup>214</sup>Pb at 37972 keV, <sup>214</sup>Pb at 38040 keV, <sup>214</sup>Pb at 38108 keV, <sup>214</sup>Pb at 38176 keV, <sup>214</sup>Pb at 38244 keV, <sup>214</sup>Pb at 38312 keV, <sup>214</sup>Pb at 38380 keV, <sup>214</sup>Pb at 38448 keV, <sup>214</sup>Pb at 38516 keV, <sup>214</sup>Pb at 38584 keV, <sup>214</sup>Pb at 38652 keV, <sup>214</sup>Pb at 38720 keV, <sup>214</sup>Pb at 38788 keV, <sup>214</sup>Pb at 38856 keV, <sup>214</sup>Pb at 38924 keV, <sup>214</sup>Pb at 39000 keV, <sup>214</sup>Pb at 39068 keV, <sup>214</sup>Pb at 39136 keV, <sup>214</sup>Pb at 39204 keV, <sup>214</sup>Pb at 39272 keV, <sup>214</sup>Pb at 39340 keV, <sup>214</sup>Pb at 39408 keV, <sup>214</sup>Pb at 39476 keV, <sup>214</sup>Pb at 39544 keV, <sup>214</sup>Pb at 39612 keV, <sup>214</sup>Pb at 39680 keV, <sup>214</sup>Pb at 39748 keV, <sup>214</sup>Pb at 39816 keV, <sup>214</sup>Pb at 39884 keV, <sup>214</sup>Pb at 39952 keV, <sup>214</sup>Pb at 40020 keV, <sup>214</sup>Pb at 40088 keV, <sup>214</sup>Pb at 40156 keV, <sup>214</sup>Pb at 40224 keV, <sup>214</sup>Pb at 40292 keV, <sup>214</sup>Pb at 40360 keV, <sup>214</sup>Pb at 40428 keV, <sup>214</sup>Pb at 40496 keV, <sup>214</sup>Pb at 40564 keV, <sup>214</sup>Pb at 40632 keV, <sup>214</sup>Pb at 40700 keV, <sup>214</sup>Pb at 40768 keV, <sup>214</sup>Pb at 40836 keV, <sup>21</sup>

greatly. For example, well and cistern salinities range from near fresh at <1–2.4 on Enewetak Island to significantly more brackish, ranging from 7 to 32 on Bikini Island. For reference, the lagoon water salinities were on average 34.6 at both atolls. The predominance of brackish groundwater is due to low rainfall recharge captured by the small island areas, which exacerbates saltwater intrusion beneath the island surfaces (Presley, 2005). The groundwater sampled with push point wells at the shore line was more saline in both locations, ranging from 26 to 29 for the Runit samples to >34.3 at Bikini Island and the islands around Bravo Crater. These brackish waters along the shore line are characteristic of the “subterranean estuary” that is an important site for mixing and exchange between land derived groundwater and the ocean (Moore, 1999). Even the shallow groundwater beneath the center of the islands is part of the subterranean estuary, since the porous coral limestone aquifer is highly permeable.

### 3.1.1. Cesium

There is a wide range of  $^{137}\text{Cs}$  activities within each atoll, with higher levels associated with groundwater and surface water in proximity to the Bravo and Mike Craters and Runit Dome (Fig. 1). More specifically, within the groundwater samples, the highest activities of  $^{137}\text{Cs}$  were found associated with either the wells at Bikini (up to  $1600\text{ Bq m}^{-3}$ ; Fig. 3a) or groundwater at the Enewetak beaches near Runit or on Enjebi Island near the Mike Crater (up to  $100\text{ Bq m}^{-3}$ ; Fig. 3d). With the exception of the Enewetak wells, which were all <  $10\text{ Bq m}^{-3}$ , the highest  $^{137}\text{Cs}$  activities were found associated with the lowest salinities, and  $^{137}\text{Cs}$  decreased with increasing salinity in the lagoon (Fig. S1 and Table S1). In the lagoons, the  $^{137}\text{Cs}$  averages were  $3.5$  and  $2.4\text{ Bq m}^{-3}$  for Bikini and Enewetak, respectively (Fig. 3a, d). These  $^{137}\text{Cs}$  activities are only a factor of 2 to 3 higher than in the open ocean outside the

lagoons or between these atolls where an average  $^{137}\text{Cs}$  activity of  $1.1\text{ Bq m}^{-3}$  was found (Table S1). Elevated (above lagoon background)  $^{137}\text{Cs}$  activities were observed in the near bottom water from the approximately 50 m deep Bravo Crater (47 m sample; Table S1), indicating a sediment source. In the shallower Mike Crater (30 m), only a slight enhancement in  $^{137}\text{Cs}$  near the bottom is seen (23 m sample; Table S1).

### 3.1.2. Plutonium

In general, there are fewer  $^{239,240}\text{Pu}$  data due to sampling and analytical constraints. Unlike  $^{137}\text{Cs}$ , there was no relationship to salinity in the combined groundwater and seawater data set (Table S1), with a wide range of  $^{239,240}\text{Pu}$  activities within the seawater and groundwater at both atolls (Fig. 2). In more detail, on Bikini the highest  $^{239,240}\text{Pu}$  activities were from a beach groundwater sample near the Bravo test site ( $820\text{ mBq m}^{-3}$ ), and a water column sample in northwest Bikini Lagoon ( $914\text{ mBq m}^{-3}$ , Fig. 3b). On Enewetak, the highest activities of  $^{239,240}\text{Pu}$  ( $1500\text{ mBq m}^{-3}$ ) were found in the lagoon just off Runit Dome (Fig. 3e), and the lowest value was from one well ( $13\text{ mBq m}^{-3}$ ) located on Enewetak Island. On average, the  $^{239,240}\text{Pu}$  activities averaged  $400 \pm 250$  and  $900 \pm 500\text{ mBq m}^{-3}$  (mean  $\pm$  std. dev.) for samples in Bikini and Enewetak Lagoons, respectively. These levels of  $^{239,240}\text{Pu}$  are more than a hundred times greater than the surface open ocean values outside the lagoons and between the atolls of around  $3\text{ mBq m}^{-3}$  (Table S1), an activity that is consistent with the broader surface North Pacific Ocean (e.g. Hirose et al., 2007).

The isotope ratios of Pu reveal clear source differences within each atoll and between the PPG and the rest of the Pacific, and more generally between PPG and global fallout in other ocean basins (Fig. 4). The Bikini Atoll samples had a  $^{240}\text{Pu}/^{239}\text{Pu}$  range of 0.17 to 0.31, with analytical errors that are quite small, varying from 0.0002 to 0.0032 (depending

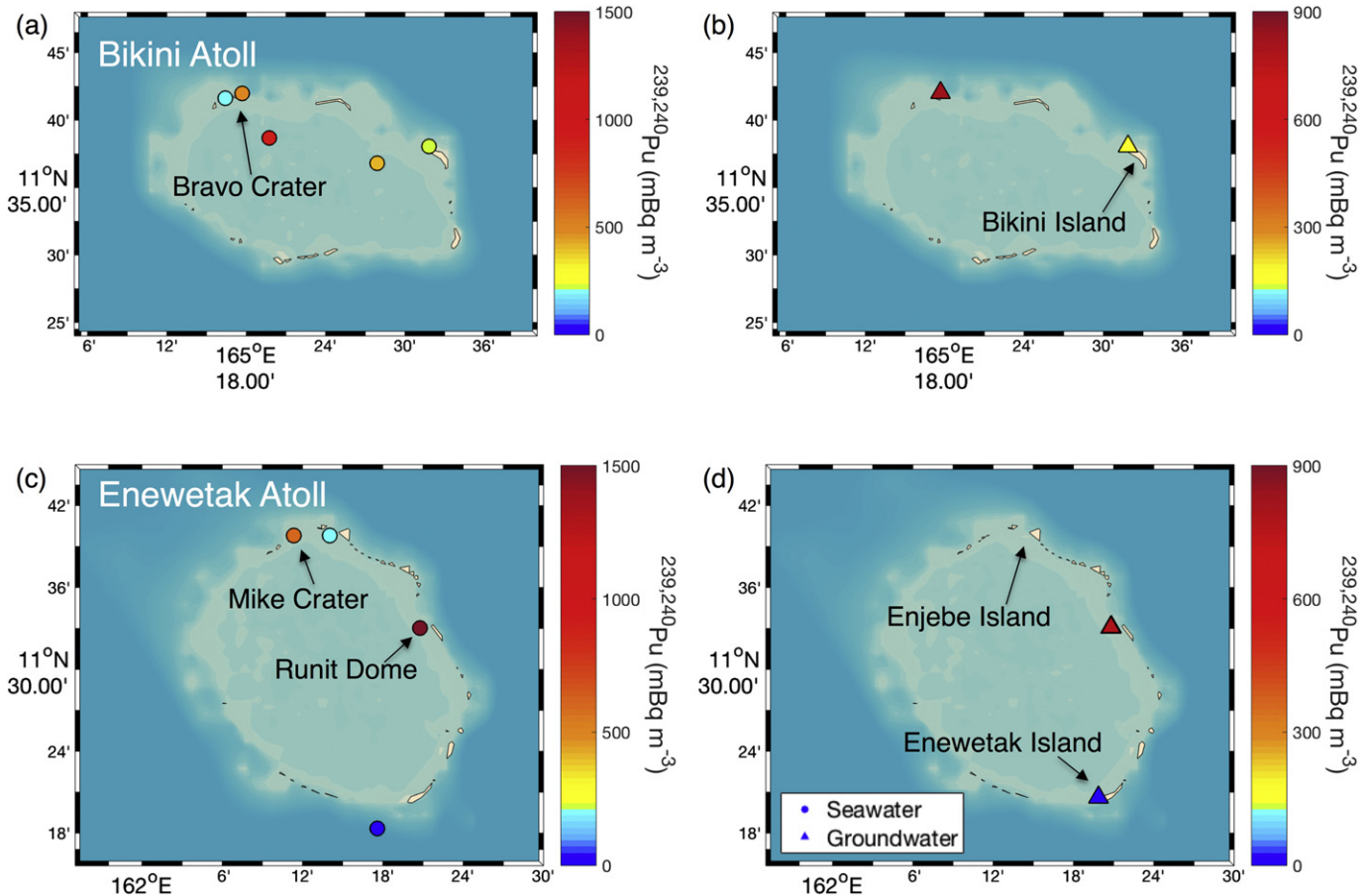
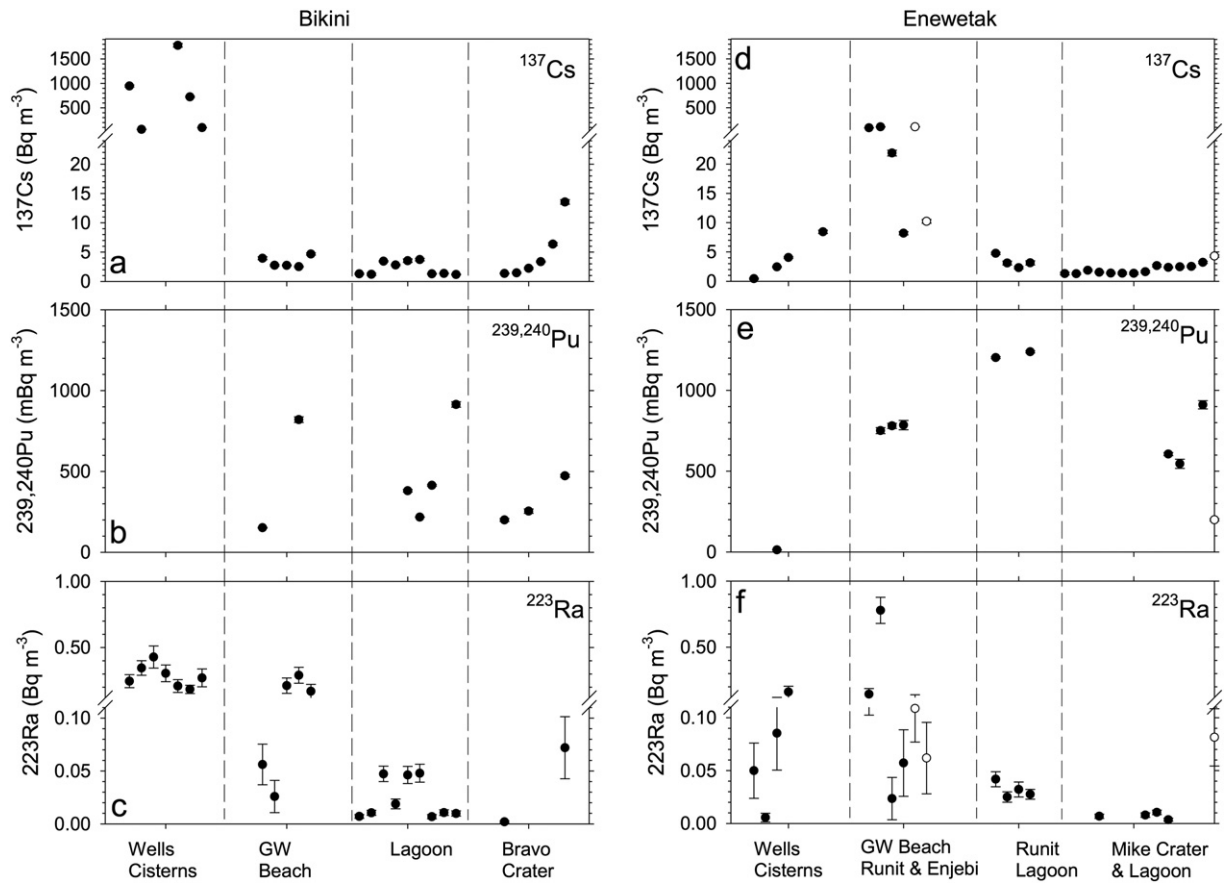
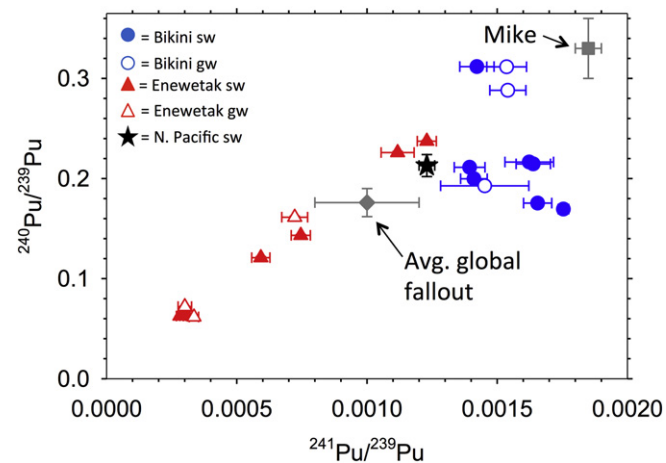


Fig. 2. Activities of  $^{239,240}\text{Pu}$  in seawater (circles) and groundwater (triangles) from Bikini (a, b) and Enewetak (c, d) atolls for both surface seawater and groundwater samples. Scales are colour coded in  $\text{mBq m}^{-3}$  as indicated.



**Fig. 3.** Comparison of  $^{137}\text{Cs}$  (a, d),  $^{239,240}\text{Pu}$  (b, e) and  $^{223}\text{Ra}$  (c, f) for Bikini (a, b, c) and Enewetak (d, e, f). Data are grouped by type with wells/cisterns on left, followed by the groundwater sampling at the shore line at the beaches (Runit and Enjebi samples distinguished by closed and open symbols, respectively). Lagoon waters are to the right for the average over the Bikini Lagoon, and specific to the Lagoon samples near Runit Dome for Enewetak. The far right set of data in each case is for the Craters at Bravo, and for Enewetak, both crater samples and the lagoon in general. All data are in Table S1 and scales are indicated on the vertical axis.

upon sample size, total Pu levels, and analytical yields). In contrast, at Bikini there was no particular trend for  $^{240}\text{Pu}/^{239}\text{Pu}$  while the  $^{241}\text{Pu}/^{239}\text{Pu}$  atom ratios were somewhat less variable, averaging  $0.0016 \pm 0.0001$  (mean  $\pm$  std. dev.).



**Fig. 4.** Atom ratios of  $^{240}\text{Pu}/^{239}\text{Pu}$  (Y axis) vs.  $^{241}\text{Pu}/^{239}\text{Pu}$  (X axis) for Bikini (blue) and Enewetak (red), with open symbols for groundwater (gw) and filled for seawater (sw) samples. Also shown for comparison are the same ratios for the Mike test (gray square, upper right), global fallout average (gray diamond) and average for a profile 800 km east of Enewetak measured in this study (black star). Error bars are shown if larger than the symbol size. Data from 2015 are in Table S1.

At Enewetak Atoll, there was a systematic difference in Pu isotopes related to the sample location in the lagoon. The lowest  $^{240}\text{Pu}/^{239}\text{Pu}$  ratios of  $0.064 \pm 0.004$  (mean  $\pm$  st. dev.) were restricted to Runit Dome groundwater and adjacent surface waters; these samples also had the highest lagoon Pu activities. This ratio increased across the lagoon from Runit in the east toward Mike Crater in the west, where it averaged  $0.225 \pm 0.013$  in the water column profile samples. A similar increase was observed for the  $^{241}\text{Pu}/^{239}\text{Pu}$  atom ratio:  $0.00030 \pm 0.00002$  near Runit to  $0.00117 \pm 0.00008$  near Mike Crater. The low ratios of both Pu isotope pairs at Runit are not commonly observed in the environment, and therefore are indicative of debris contaminated by a unique source of Pu, most likely from the failed Quince test in 1958. During this “dud” test, there was no fission derived neutron flux required to produce the higher mass Pu isotopes, but wide local contamination from the conventional explosive trigger (Noshkin and Robison, 1997). At the same location, a second low-yield test named Fig further disturbed the soil and left behind a heterogeneous debris field (Hamilton et al., 2009). There were several tests on or around Runit Island, many of which were low yield, thereby contributing to the low Pu isotope ratios still present today in the Runit Dome area.

### 3.1.3. Radium

Radium isotopes were generally highest in the wells, and elevated in groundwater at the shoreline compared to the lagoons (Table S1, Fig. 3c, f). In seawater,  $^{223}\text{Ra}$  was highest in the surf zone samples and was inversely correlated with tidal stage in a water column time series collected at the dock on Bikini Island (Fig. S2). This pattern is consistent with a groundwater source driven by tidal pumping (Burnett et al., 2008; Santos et al., 2009). Furthermore,  $^{223}\text{Ra}$  activities in the surf

zones at Bravo and Enjebi Islands were the most elevated seawater samples at Bikini and Enewetak Atolls, respectively, including a surf zone sample from the Bravo Crater with elevated  $^{137}\text{Cs}$  (Fig. 3c). Together, these data are suggestive of a significant control on radionuclide activities driven by sediment-water exchange processes.

### 3.2. Seafloor sediments

The range in sediment activities is large between sites on the seafloor (Fig. 5; all sediment data in Table S2). By far the highest sediment activities were found in cores from the Bravo and Mike Craters, where we were able to sample down to 80 and 62.5 cm, respectively. When calculating inventories of these radionuclides it must be assumed that there is activity below the depth of sampling, here below 60 to 80 cm in the craters, hence we can only provide minimum estimates. This limits our assessment not just in the craters, but off Runit Dome (32 cm core), where a prior study found artificial radionuclides as deep as 2 m below the seafloor (McMurtry et al., 1986).

Our highest vertical resolution data are from gamma spectroscopy for which  $^{137}\text{Cs}$  and  $^{241}\text{Am}$  were readily quantifiable, and in one location in particular, for  $^{207}\text{Bi}$  as well (Bravo Crater, discussed below). Profiles

were mostly uniform for  $^{137}\text{Cs}$ , and ranged from 100 to 200  $\text{Bq kg}^{-1}$  in the craters, to only 1–5 in the other cores from the shorelines of Bikini Island and Runit Dome (Fig. 5a).  $^{241}\text{Am}$  is present in even higher abundances than  $^{137}\text{Cs}$  in the sediment cores at activities up to 3200  $\text{Bq kg}^{-1}$  (Fig. 5b).

Selected sediment samples were quantified for Pu isotopes; the craters with the highest  $^{241}\text{Am}$  also had the highest total  $^{239,240}\text{Pu}$  activities (Fig. 5c). The high activity samples also had some of the highest ratios of  $^{240}\text{Pu}/^{239}\text{Pu}$ , consistent with the large thermonuclear tests that resulted in higher local activities and greater production of the heavy Pu isotopes as discussed above for the water column results. Sediments off Runit Dome were characterized by low  $^{240}\text{Pu}/^{239}\text{Pu}$  atom ratios of 0.064 (Fig. 5c), identical to the waters in the lagoon in that area and in the groundwater originating from Runit Dome. While the sediments off Runit Dome were not as high as the craters for the activity of total sediment bound Pu, the low Pu isotope ratio in the Runit Dome area makes it possible to track this unique source in Enewetak Lagoon (see Discussion).

Though not a focus of this study, the Bravo Crater sediments contained  $^{207}\text{Bi}$  ( $t_{1/2} = 32.2$  y), with activities up to 2500  $\text{Bq kg}^{-1}$  (Fig. 5d). This isotope was not detected elsewhere other than at low

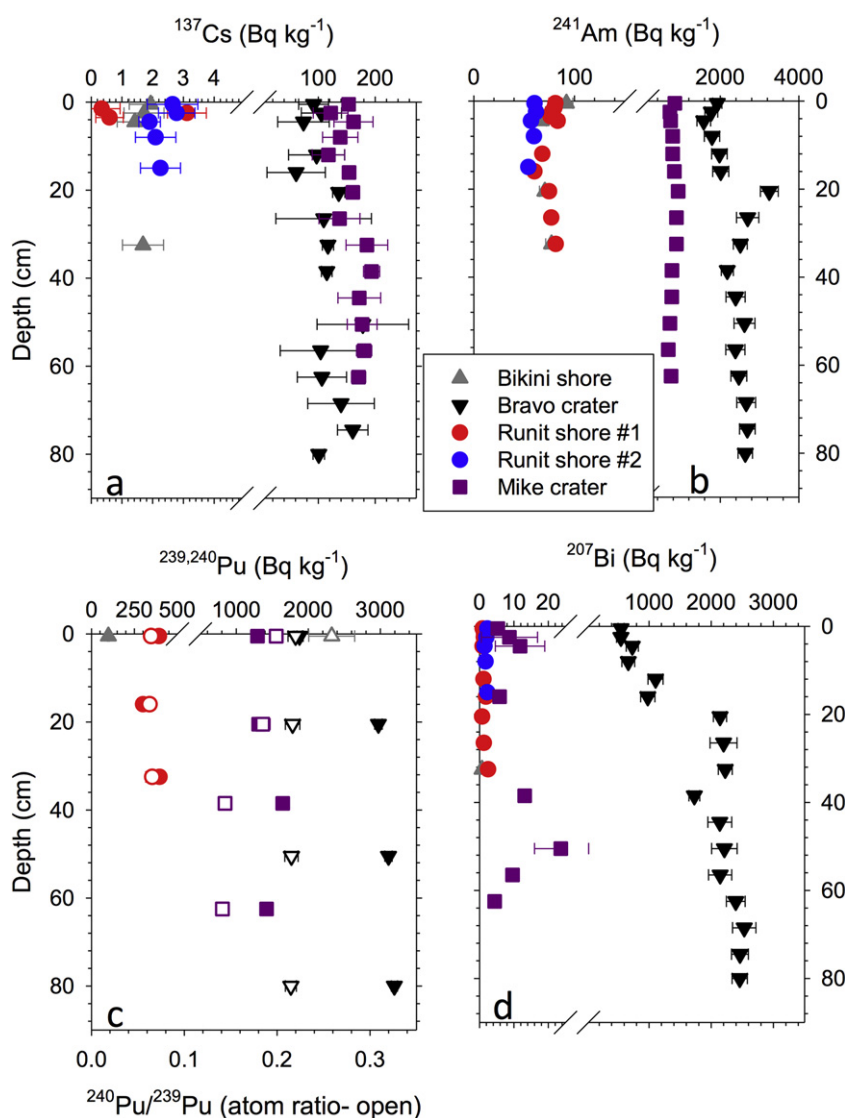


**Fig. 5.** Sediment core profiles vs. depth (cm-Y axis) for  $^{137}\text{Cs}$  (a),  $^{241}\text{Am}$  (b),  $^{239,240}\text{Pu}$  (c) and  $^{207}\text{Bi}$  (d). For each radionuclide the activities are along the upper x-axis in units of  $\text{Bq kg}^{-1}$  dry weight. For Pu, also shown are the  $^{240}\text{Pu}/^{239}\text{Pu}$  atom ratios as open symbols with scale along the lower x-axis. Sample key is shown for Bikini shore (gray triangles), Bravo Crater (black inverted triangles), Runit shore (#1 and #2 are two sites, red and blue circles, respectively) and the Mike Crater (purple square). Error bars are shown if larger than the symbol size for each measurement. Data are in Table S2.

levels at a few depths in sediments from Mike Crater ( $<25 \text{ Bq kg}^{-1}$ ). There has been some speculation on the origin of  $^{207}\text{Bi}$ , not commonly measured due to its low abundance in global fallout, and thought to be sourced from a specific nuclear weapon design tested in 1958 (Bossew et al., 2006).

## 4. Discussion

### 4.1. Seawater and groundwater activities

Our results demonstrate a large contrast between Cs and Pu activities, namely that  $^{137}\text{Cs}$  is highest in groundwater and not particularly elevated in the lagoon, whereas  $^{239,240}\text{Pu}$  remains elevated in the groundwater samples from the shoreline and the lagoon proper, relative to the surrounding ocean (Figs. 1 and 2). This finding is similar to prior studies where the elevated Pu activities in the atoll lagoons were considered a source indicator for Pu from the PPG to the broader Pacific (Buesseler, 1997; Kim et al., 2004; Noshkin and Wong, 1979; Pittauer et al., 2017; Wu et al., 2014). Hence, these new data, collected in 2015, indicate that the PPG remains a source of anthropogenic radioactivity today, albeit a small one relative to the large inventory in the ocean that remains from earlier atmospheric fallout. The sources of these radionuclides to the atoll lagoon water columns as well as their export to the Pacific Ocean via lagoon flushing are discussed in more detail below.

Within the atolls, the activity levels of  $^{137}\text{Cs}$  and  $^{239,240}\text{Pu}$  varied substantially within the lagoon waters depending upon location, increasing near known sources, such as for Pu in lagoon waters near Runit Dome or for Cs in the Bravo Crater deep waters. We summarize the differences

not only between these locations in 2015, but in comparisons to studies in the 1970's of the Marshall Islands, and on a larger scale, relative to modern global surface ocean averages in Fig. 6 (units of  $\text{Bq m}^{-3}$  for  $^{137}\text{Cs}$  and  $\text{mBq m}^{-3}$  for  $^{239,240}\text{Pu}$ ; data and references in Table 1). We present the data as of 2015, decay correcting  $^{137}\text{Cs}$  data from the earlier studies in the 1970s to 2015, so that the differences in activity levels reported here are due to a loss term or continued source and not due to radioactive decay alone. For  $^{137}\text{Cs}$  this results in a decrease in activity by 60% in 40 years since the mid-1970s to 2015 due to decay ( $^{239}\text{Pu}$  and  $^{240}\text{Pu}$  decay corrections are negligible).

Looking first at the surface seawater data,  $^{137}\text{Cs}$  activities are elevated over the global ocean average by only a factor of two within the Bikini and Enewetak Lagoons, including waters near Runit Dome and above the Bravo and Mike Craters (averages shown in Fig. 6). In our data, the only significant deviations for  $^{137}\text{Cs}$  for water samples are near the seafloor at Mike Crater and in groundwater of brackish salinities (Fig. 1, Fig. S1). Comparing current  $^{137}\text{Cs}$  levels at Bikini and Enewetak to the past is complicated by variability within the lagoon waters, but a systematic sampling of over 200 samples during several field campaigns in the 1970s (see Table 2 in Robison and Noshkin, 1999), resulted in a well-documented average for both lagoons of  $4\text{--}6 \text{ Bq m}^{-3}$  (again decay corrected to 2015). Thus to the degree we have representatively sampled the lagoons in 2015, levels of  $^{137}\text{Cs}$  are a factor of two lower in 2015 after 40 years. This observed decrease is constant with earlier studies suggesting a decrease of  $^{137}\text{Cs}$  in the lagoons due to its relatively rapid remobilization from the seafloor (Hamilton et al., 1996; Noshkin and Wong, 1979), and a diminishing source from island aquifer runoff (Robison et al., 2003). More samples would be needed to confirm this

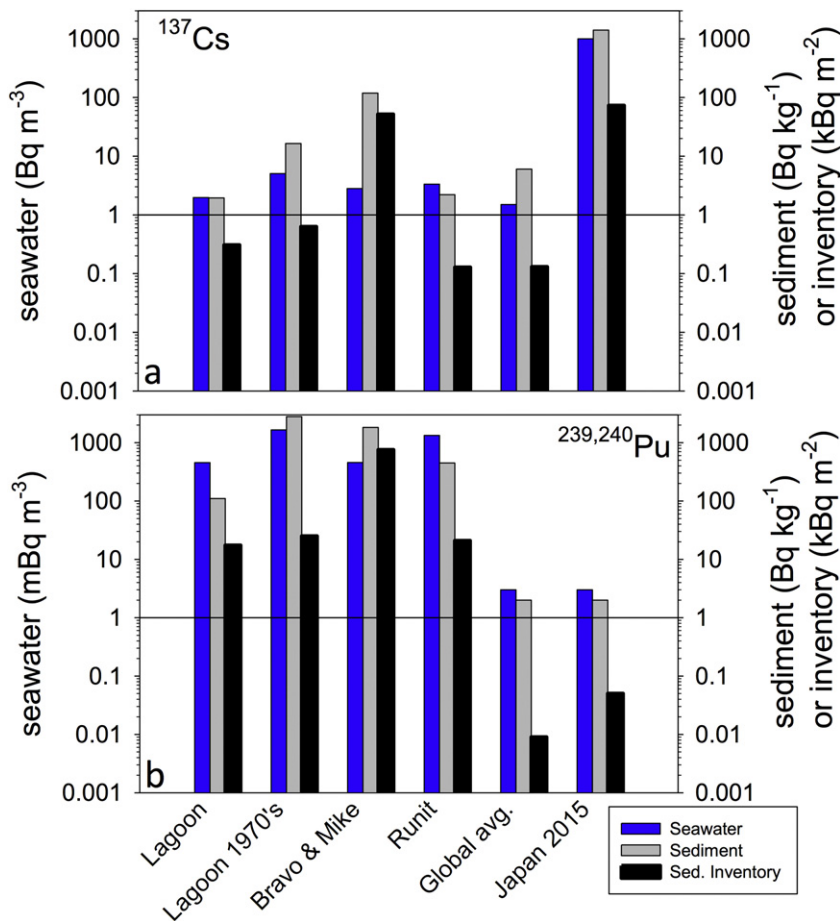


**Fig. 6.** Comparison of  $^{137}\text{Cs}$  (a) and  $^{239,240}\text{Pu}$  (b) between the average values measured in seawater (blue), sediment (gray) and the sediment inventory (black). Note log scale and units on X-axis. The data from this study have been averaged for the lagoon waters of both Bikini and Enewetak (outside of hot spots), the Runit Dome area, and the Bravo and Mike Craters. The 2015 lagoon data are compared to lagoon averages for the 1970's and compared to an ocean global average, as well as the waters and seafloor near the Fukushima Dai-ichi nuclear power plant as sampled in 2015. All data in Table 1.



**Table 1**  
Summary of  $^{137}\text{Cs}$  and  $^{239,240}\text{Pu}$  in Marshall Islands vs. other locations and times.

	$^{137}\text{Cs}$			Pu			Pu/Cs			
	Water	Sediment	Sediment inventory	Water	Sediment	Sediment inventory	Water	Sediment	Sediment inventory	Sed/water
	Bq/m <sup>3</sup>	Bq kg <sup>-1</sup>	kBq/m <sup>2</sup>	mBq/m <sup>3</sup>	Bq kg <sup>-1</sup>	kBq/m <sup>2</sup>	Bq/Bq	Bq/Bq	Bq/Bq	
Enewetak and Bikini lagoons	2.0	1.9	0.31	455	99	16	0.23	51	51	221
Runit Dome area	3.3	2.2	0.13	1331	393	20	0.40	178	158	446
Bravo and Mike Craters	2.8	119	52	457	1586	856	0.16	13	17	82
Lagoon avg. 1970's	5.0	16	0.63	1650	2800	25	0.33	171	40	520
Global ocean average	1.5	6.0	0.13	3	2	0.01	0.002	0.333	0.069	167
Japan near FDNPP 2015	1000	1400	73	3	2	0.1	3.0E-06	0.0014	0.0007	476

Lagoon, Runit, Bravo and Mike Craters are averages from 2015 from this study. Sediments from lagoon are from this study and 1970's from Bikini only.

Lagoon water avg. 1970's from Robison and Noshkin (1999).

Lagoon sediment avg. 1970's from Noshkin et al. (1997a, 1997b) (part 3) & Robison and Noshkin, 1999.

Global sediment inventory are global fallout estimates decay corrected for cesium-137 decay.

Japan water data from Buesseler et al., 2017 and references therein.

Japan sediment data from Black and Buesseler 2014 and references therein.

given expected variations due to local currents and mixing within the lagoons and with surrounding waters.

For  $^{239,240}\text{Pu}$  in seawater, activities at Bikini and Enewetak are many hundreds of times higher relative to the surface global ocean average (Fig. 6). This holds for all locations sampled within the lagoons, though levels of Pu are about 2 to 3 times higher near the Runit Dome than elsewhere at Enewetak. We also note a  $\approx 3$ -fold decrease in  $^{239,240}\text{Pu}$  activities over the past 40 years, dropping from an average of 1650 Bq m<sup>-3</sup> for both lagoons in the 1970's (Robison and Noshkin, 1999) to below 500 Bq m<sup>-3</sup> in 2015. As with Cs, seawater Pu activities will be controlled by sediment inputs and exchange with lower activity waters outside the lagoon; however, Pu has a significantly higher affinity for particle surfaces, hence scavenging removal of Pu also plays a role. In the North Pacific Ocean, the highest Pu levels are in a subsurface maximum (>100 to 1000 m), formed during remineralization of surface-scavenged Pu on sinking particles (Bowen et al., 1980; Lindahl et al., 2010). Within the Pu maximum, Pu activities are thought to be decreasing due to long term scavenging: subsurface activities of  $\approx 100$  mBq m<sup>-3</sup> had decreased by half in the North Pacific by the turn of the century (Hirose et al., 2009). Here, in a single 6 point profile northwest of the Marshall Islands we measured a maximum  $^{239,240}\text{Pu}$  of 31 Bq m<sup>-3</sup> at 950 m at 16° N 156.8° E (Table S1). Regardless, all of the Bikini and Enewetak seawater Pu activities exceed the Pu values in the rest of the ocean, supporting the idea that the atolls remain a net source of Pu to the North Pacific.

#### 4.2. Seafloor sediments

For the seafloor, it is illustrative to compare Cs and Pu to other sites and times by looking at either the surface sediment average activities (Bq kg<sup>-1</sup>, typically 0–2 cm) or the inventory for an entire core (Bq m<sup>-2</sup>, Fig. 6). Notably, Pu levels in all sediment samples are orders of magnitude higher than other ocean settings. For Cs, the sediment enrichment is largely confined to the Bravo and Mike craters (Fig. 6, Table 2). For example, average sediment for  $^{239,240}\text{Pu}$  activities in the top of the cores are 110 and 1820 Bq kg<sup>-1</sup>, for the lagoon and craters,

respectively and 2 and 120 Bq kg<sup>-1</sup> for  $^{137}\text{Cs}$ . The average lagoon core top activities in the 1970s were also higher, at 2800 Bq kg<sup>-1</sup> for  $^{239,240}\text{Pu}$  and 16 Bq kg<sup>-1</sup> for  $^{137}\text{Cs}$  (decay corrected to 2015) (Noshkin et al., 1997a; Noshkin et al., 1997b; Robison and Noshkin, 1999), though again the large spatial variability complicates making simple comparisons over time without more comprehensive sampling today. Sediment inventories also show large differences, being most enriched in the craters (Table 2) where they are much higher than expected from global fallout. As noted earlier however, the cores collected here did not reach background radionuclide abundances, so they are by default a minimum estimate of total radionuclide inventory associated with the seafloor. Earlier studies included high spatial sampling resolution across the lagoon (>50 sites sampled in 1979 – Noshkin et al., 1997a, 1997b), but they also routinely sampled only to 16 cm, missing the high activities we see extending down to >80 cm for example in the Mike Crater.

Americium-241 is essentially absent from fresh nuclear weapons debris but is produced thereafter as a result of the decay of  $^{241}\text{Pu}$ . Thus it is elevated at the sites of the highest yield tests where the heavier isotopes of Pu were preferentially produced. In most seafloor sediments,  $^{241}\text{Am}$  activities are too low to detect via gamma spectroscopy, but the sediments of Bikini and Enewetak are exceptional in that regard with activities > 1000 Bq kg<sup>-1</sup> in the Mike and Bravo craters. Over longer time scales the decay loss associated with  $^{241}\text{Am}$ 's 432 year half-life will become increasingly important, resulting in a predicted peak in  $^{241}\text{Am}$  in the environment in 2037 (Krey et al., 1976).

There has been some speculation on the origin of  $^{207}\text{Bi}$ , as it is rarely detected in global fallout (Bossey et al., 2006). Its origin is not proportional to the test yield, but rather the specific design of the nuclear weapon. While there may be more than one mechanism to generate  $^{207}\text{Bi}$ , its presence is most likely due to activation with neutrons of stable bismuth, or possibly lead used in the weapons design of so called "clean devices" where most of the blast energy is derived from fusion (Noshkin et al., 2001). Noshkin suggested that the bulk of the PPG  $^{207}\text{Bi}$  was produced as a consequence of one such specific test named Poplar in July 1958 conducted in the Bravo Crater. However, there were additional tests in the same crater; hence the core activities and isotope ratios

**Table 2**  
Summary Table Inventories (Bq/m<sup>2</sup>).

	Sampling date	Approx. depth	Lat N	Lon E	Core length cm	$^{137}\text{Cs}$		$^{239,240}\text{Pu}$		$^{241}\text{Am}$		$^{207}\text{Bi}$	
						0–2 cm	Whole	0–2 cm	Whole	0–2 cm	Whole	0–2 cm	Whole
Bikini shore	19-Jan-15	6	11.6287	165.5194	34	29	306	1479		1272	13,900	BD	
Bravo	20-Jan-15	50	11.6981	165.2715	81	3192	49,593	65,277	1,229,737	60,565	1,016,186	17,893	773,281
Runit shore #1	23-Jan-15	6	11.5493	162.3445	37	21		4767		891	22,565	15	376
Runit shore #2	23-Jan-15	3	11.5493	162.3445	20	17	128	3808	19,756	379	6293	14	234
Mike	24-Jan-15	30	11.6633	162.1888	64	1182	53,951	133	6036	6610	263,648	58	3706

All inventories in Bq/m<sup>2</sup>.

will be a blend of these local events. Given its 32 year half-life, 60% of the  $^{207}\text{Bi}$  measured in a core from Bravo Crater in 1972 by Noshkin would have decayed by 2015, resulting in predicted  $^{241}\text{Am}/^{207}\text{Bi}$  ratios from 1.65 to 0.6 from the top to bottom, respectively of their 72 cm Bravo core (calculated from Table 3 in Noshkin et al., 2001). Our  $^{241}\text{Am}/^{207}\text{Bi}$  ratios range from 3.5 to 1.1, suggesting to first order that the loss of  $^{207}\text{Bi}$  is occurring twice as fast as  $^{241}\text{Am}$  from these sediments.

The radionuclides profiles all tend to have little vertical structure with the exception of  $^{207}\text{Bi}$ , which may differ due to its unique source from a single test. There are several processes that will redistribute radionuclides in sediments, including bioturbation and physical mixing that has happened either since the blasts, or as a consequence of the blasts themselves. For example, McMurtry et al. (1986) found evidence of bioturbation down to 2 m in core collected at Enewetak. Activities can be reduced over time by burial of more recent, less contaminated materials, though this process typically occurs over longer time scales, and the craters would be deposition centers for contaminated material that has been resuspended from other areas of the lagoons. Net losses from the sediment to the water column are possible due to physical re-suspension of sediments, or exchange with pore waters and subsequent diffusive losses that may be enhanced by bio-irrigation (McMurtry et al., 1986). This is not a study of the details of these processes, though whole core inventories are not directly impacted by sediment mixing, so they are informative to consider if seeking to detect long term sources or sinks. Regardless, incomplete sampling of lagoon sediment inventories at Bikini and Enewetak remain a large uncertainty in assessing what remains today from weapons testing activities during the middle of the last century.

#### 4.3. Comparisons to levels off Japan due to Fukushima Dai-ichi nuclear power plants

We can also compare what we measured in Bikini and Enewetak in 2015 to the ocean setting near the Fukushima Dai-ichi nuclear power plants (FDNPPs), which in 2011 became the largest accidental source of radionuclides to the ocean. The highest  $^{137}\text{Cs}$  activities in 2015 in the surface ocean were found near FDNPP (Fig. 6a) where samples closest to FDNPP had an average  $^{137}\text{Cs}$  level around  $1000 \text{ Bq m}^{-3}$  even 4 years after initial releases, which peaked with  $^{137}\text{Cs} > 50$  million  $\text{Bq m}^{-3}$  in the surface ocean in early June 2011 (Buesseler et al., 2011). The levels of  $^{137}\text{Cs}$  in these atolls are nowhere near as high as measured off Japan (Buesseler et al., 2017). Unlike the highly elevated Cs levels off FDNPP, the  $^{239,240}\text{Pu}$  levels off Japan are indistinguishable from the global fallout average (Fig. 6b), as the release ratios of  $^{137}\text{Cs}/\text{Pu}$  in that accident were greater than a million to one (Steinhauser, 2014; Zheng et al., 2013).

#### 4.4. Pu isotope ratios and the Runit dome area

Plutonium isotope ratios will differ based upon the fraction of local fallout and ongoing sources of Pu from each of the 66 nuclear tests at Bikini and Enewetak. At Bikini and Enewetak, Pu atom ratios are much more variable than for areas impacted by global fallout; in the Northern Hemisphere,  $^{240}\text{Pu}/^{239}\text{Pu}$  and  $^{241}\text{Pu}/^{239}\text{Pu}$  averages are quite constant at  $0.180 \pm 0.007$  and  $0.00094 \pm 0.00007$ , respectively (gray diamond, Fig. 4) (Kelley et al., 1999). Lower ratios of both are more typical of weapons grade material and low yield detonations, such as at the Nevada test site, which was characterized by a fallout  $^{240}\text{Pu}/^{239}\text{Pu}$  ratio of 0.035 (Buesseler, 1997; Hicks and Barr, 1984). Higher Pu ratios can be attributed to the 1952 Mike thermonuclear test, as documented in corals (Buesseler, 1997; Froehlich et al., 2016; Lachner et al., 2010; Lindahl et al., 2011; Noshkin et al., 1975). In early samples of airborne debris and fallout from the Mike test, Diamond et al. (1960) measured a  $^{240}\text{Pu}/^{239}\text{Pu}$  atom ratio of 0.30–0.36 and a  $^{241}\text{Pu}/^{239}\text{Pu}$  atom ratio of  $\sim 0.0019$  if decay corrected to 2015 (using the original  $^{241}\text{Pu}/^{239,240}\text{Pu}$  activity ratio of 27 as reported in Diamond et al., 1960; Fig. 4, gray

square). These Pu ratios were similar to ash collected after the 1954 Bravo thermonuclear test from the Japanese fishing boat “Lucky Dragon” (“Fukuryu-Marun” (“Lucky Dragon” in English), which was at sea near the testing site when the bomb was detonated (Hisamatsu and Sakanoue, 1978).

As a consequence of the high ratio and high yield tests that deposited considerable close-in fallout, the North Pacific has higher than average  $^{240}\text{Pu}/^{239}\text{Pu}$  atom ratios ( $> 0.2$ ). This elevated ratio over global fallout is used as a tracer for PPG derived Pu at sites as far away as the Seas around China, Korea and Japan (Kim et al., 2004; Wu et al., 2014; Zheng et al., 2013). Not only are the ratios higher due to PPG sources, but the ratios increase with depth in the ocean and in the seafloor sediments of the North Pacific, consistent with a more rapidly removed form of fallout Pu due to incorporation of the coral debris characteristic of close-in fallout (e.g. Buesseler, 1997). Plutonium isotope ratios we measured from a profile 800 km west of Enewetak (Fig. 4, star) confirm that this mix of global fallout and PPG sources in the North Pacific is observed in the open ocean outside of the Marshall Islands.

Within the atoll lagoons, the story is a bit more complicated. In Enewetak lagoon, the Pu isotopic data suggest conservative mixing between two endmembers (red triangles, Fig. 4). One endmember appears to be related to Pu sources in the vicinity of the Runit Dome, where seawater, groundwater and sediments have a  $^{240}\text{Pu}/^{239}\text{Pu}$  ratio of  $0.065 \pm 0.003$ . The other originates in the waters above Mike Crater, with ratios that average  $0.225 \pm 0.013$ . Seawater  $^{240}\text{Pu}/^{239}\text{Pu}$  ratios within the Enewetak lagoon fall along a mixing line between these two sources. At Bikini, the trend is quite different in that the Pu isotope ratios do not follow simple two end member mixing, but are all elevated with  $^{240}\text{Pu}/^{239}\text{Pu} > 0.22$  and  $^{241}\text{Pu}/^{239}\text{Pu}$  ratios  $> 0.0014$  (blue circles, Fig. 4).

For Enewetak, we can use this linear trend in isotope ratios to predict the fraction of Pu coming from two different sources (Buesseler and Sholkovitz, 1987; Krey et al., 1976):

$$\frac{[\text{Pu activity}]_1 / [\text{Pu activity}]_2 = (R_2 - R) / (R - R_1)}{* (1 + 3.67R_1) / (1 + 3.67R_2)} \quad (1)$$

where R is the measured  $^{240}\text{Pu}/^{239}\text{Pu}$  atom ratio in the sample and  $R_1$  and  $R_2$  are the ratios in the two end members. The factor of 3.67 converts from atom ratios to the relative activities of  $^{239,240}\text{Pu}$  from both sources. Using for  $R_1$  the 0.065 Runit Dome area and for  $R_2$  the 0.225 Mike Crater  $^{240}\text{Pu}/^{239}\text{Pu}$  atom ratio endmembers, compared to the two mid lagoon samples with an average  $^{240}\text{Pu}/^{239}\text{Pu}$  atom ratio of 0.132, results in an estimate that 48% of the  $^{239,240}\text{Pu}$  in the lagoon waters is derived from the Runit Dome area source and 52% from waters originating from the Mike Crater area. Thus, Pu from the larger tests near Mike Crater and that associated with the Runit Dome area are contributing equally to Pu activities in the Enewetak lagoon water column.

This calculation is sensitive to the chosen end-members, and while the Runit Dome area low ratio is rather well constrained here, the Mike source ratio, if pure, would be closer to 0.33 or higher. In that case, about 62% of the Pu in the lagoon seawater would be derived from the Runit area source. The high Pu ratio cannot be lower than observed in the lagoon samples (0.225), which would set the bounds on the Runit area source contribution in the range of 50–60%. Further, while there might be  $> 2$  endmembers, the consistency of the mixing line for both Pu isotope pairs in Enewetak surface waters, strongly suggests that the system Pu inputs are dominated by two sources and that about half of the Pu in the lagoon originates from the Runit Dome area.

This finding is surprising as the total amount of  $^{239,240}\text{Pu}$  associated with the material buried beneath the dome is estimated to be  $< 1\%$  of the total inventory of  $^{239,240}\text{Pu}$  at Enewetak Atoll (Noshkin and Robison, 1997). This includes the waste disposal estimates for Pu buried intentionally beneath the dome, as well as the Pu in the sediments within 1 km surrounding the dome (Davisson et al., 2012; Noshkin and Robison, 1997). Our sediment inventory data generally support this latter point, with the  $^{239,240}\text{Pu}$  inventory in our single Runit Island core being 1.6%

of the inventory we measured in the Mike Crater core (Table 2), with the caveats that we did not conduct a comprehensive sampling of the seafloor, nor did our cores reach below the deepest layers of contamination. More comprehensive seafloor sampling with deeper cores in the Runit area may reveal higher inventories, but with the data in hand we conclude that while the fraction of total Pu associated with the Runit Dome area sediments is small, it contributes disproportionately to the total Pu flux to the lagoon waters (discussed further in Section 4.6).

We know of no other study with similar  $^{240}\text{Pu}/^{239}\text{Pu}$  data in the lagoon waters for comparison. However, this finding is supported by a recent study of marine biota on Enewetak that documented  $^{240}\text{Pu}/^{239}\text{Pu}$  ratios as low as  $0.07 \pm 0.01$  in sea cucumbers, clams and snails living in the waters between Runit Dome and as high as 0.22–0.26 in specimens off Enjebi Island near Mike Crater (Hamilton et al., 2008). In that study it was suggested that the Pu isotope ratios might provide a useful tracer to monitor source term attribution for Pu in biota, and the same appears to be true for surface waters in this lagoon.

#### 4.5. Total fluxes of cesium and plutonium from the atoll lagoons

At Bikini and Enewetak Atolls, both  $^{239,240}\text{Pu}$  and  $^{137}\text{Cs}$  are enriched in lagoon seawater relative to samples collected outside the lagoon inlets. Therefore, the atoll lagoons must be a net source of both Pu and Cs to the North Pacific Ocean. At steady-state, the total flux of Pu and Cs from the lagoons can be calculated as:

$$F = (A_{\text{lagoon}} - A_{\text{Pacific}}) * V / T_W \quad (2)$$

where  $F$  is the flux ( $\text{Bq d}^{-1}$ ) of  $^{239,240}\text{Pu}$  or  $^{137}\text{Cs}$ ,  $A$  is the activity of  $^{239,240}\text{Pu}$  or  $^{137}\text{Cs}$  in seawater inside (lagoon) or outside (Pacific) the lagoon,  $V$  is the volume of the lagoon ( $\text{m}^3$ ), and  $T_W$  (d) is the residence time of seawater within the lagoon. This latter term ( $T_W$ ) is derived using Ra isotopes, which are input to the lagoon water column through submarine groundwater discharge (SGD). Once the Ra isotopes are released in to seawater, their distribution is controlled only by mixing and decay (Moore, 2000). By normalizing to the activity of a long-lived Ra isotope (here,  $^{226}\text{Ra}$ ) to account for loss via mixing, the short-lived Ra isotope (here,  $^{223}\text{Ra}$ ) can be used to quantify water mass age, a proxy for  $T_W$  (e.g. Charette et al., 2013). The residence time model and assumptions are described in detail in the Supplementary Material.

The lagoon residence times for Bikini and Enewetak Atolls were determined from Ra to average 36 and 16 days, respectively (Fig. S3). These estimates are broadly consistent with lagoon flushing time estimates based on independent techniques. For example, using a combination of field measurements and a to-scale lab model, von Arx (1948) derived a wintertime average Bikini lagoon residence time of 39 days. Atkinson et al. (1981) used a circulation-based box model to determine that Enewetak lagoon has a residence time of 28 days.

Using the respective  $A_{\text{lagoon}}$  and  $A_{\text{Pacific}}$  values for  $^{239,240}\text{Pu}$  or  $^{137}\text{Cs}$ , lagoon volumes, and Ra-derived  $T_W$  estimates, we determined the lagoon export fluxes ( $F$ ) of each radionuclide for Bikini and Enewetak Atolls (Table S3). For Bikini, radionuclide fluxes were determined to be  $6.6 \times 10^8 \text{ Bq d}^{-1}$  and  $3.3 \times 10^8 \text{ Bq d}^{-1}$  for  $^{239,240}\text{Pu}$  and  $^{137}\text{Cs}$ , respectively. At Enewetak, we estimate that the fluxes are close to an order of magnitude higher, at  $2.2 \times 10^9 \text{ Bq d}^{-1}$  and  $1.5 \times 10^9 \text{ Bq d}^{-1}$  for  $^{239,240}\text{Pu}$  and  $^{137}\text{Cs}$ , respectively. This difference is driven by a combination of slightly higher radionuclide inventories and the shorter residence time of the Enewetak Atoll lagoon.

Noshkin and Wong (1979) used the difference in Pu activities within the lagoon and outside and a residence time of 144 days to calculate steady-state fluxes of 0.085 and 0.12  $\text{TBq yr}^{-1}$  for  $^{239,240}\text{Pu}$  for Enewetak and Bikini, respectively. Their estimates increased to 0.4 to 0.6  $\text{TBq yr}^{-1}$  for Enewetak and Bikini, respectively, if using the assumption of a shorter 30 day residence time. These latter estimates, which used a residence time similar to our study, are in good agreement with our annualized Bikini and Enewetak  $^{239,240}\text{Pu}$  fluxes of 0.2 and 0.8  $\text{TBq yr}^{-1}$ ,

respectively. Therefore, it appears that to first order, the total lagoon export fluxes are largely unchanged at least since the 1970s. As noted earlier, the elevated  $^{240}\text{Pu}/^{239}\text{Pu}$  ratios in the Pacific are attributed to close-in fallout that was generated largely by the high yield thermonuclear tests. Bowen et al. (1980) estimate that the PPG delivered on the order of 3.8 PBq of  $^{239,240}\text{Pu}$  and 56 PBq of  $^{137}\text{Cs}$  to the N. Pacific as a consequence of close-in fallout, using their measured inventories of Pu and Cs in the water column and delivery estimates of global fallout at these latitudes. This far exceeds the amount of Pu and Cs that has been added via the ongoing releases from the Bikini and Enewetak lagoons, which if continuous over the past 60 years, would total only 0.03 PBq for  $^{239,240}\text{Pu}$  (using an average flux of 0.5  $\text{TBq yr}^{-1}$ ), and 0.02 PBq  $^{137}\text{Cs}$  (using an average flux of 0.3  $\text{TBq yr}^{-1}$ ). Thus the elevated  $^{240}\text{Pu}/^{239}\text{Pu}$  ratios in the broader N. Pacific are consistent with the close-in fallout dominated by earlier high yield testing, and not the smaller ongoing flux of Pu from the Marshall Islands, which at least at Enewetak, is characterized by on average lower  $^{240}\text{Pu}/^{239}\text{Pu}$  ratios.

#### 4.6. Groundwater fluxes as a source of marine artificial radioactivity

The calculation of total exchange rates of Pu and Cs from the lagoons does not tell us if the source of radioactivity is coming from the seafloor via desorption and exchange with pore waters or from SGD sources from the islands surrounding the atoll. Radium isotopes allow us to quantify the SGD source for both Bikini and Enewetak, which we can estimate via a mass-balance model and measured Ra activities (Supplementary Material). In particular at Enewetak, our Ra groundwater data can uniquely help determine if the low  $^{240}\text{Pu}/^{239}\text{Pu}$  ratio source associated with the Runit Dome area is derived from the exchange of groundwater underneath the unlined dome, or from porewater and other exchange mechanisms with Pu buried in the lagoon. This is an important question for those trying to resettle on these islands (Council, 1982; Gerrard, 2015).

From the time-series Ra isotope measurements at Bikini and Runit Islands combined with groundwater Ra isotope activities from island wells, we found SGD averages ( $\pm$  std. error) of  $3.3 \pm 1.3 \text{ cm d}^{-1}$  and  $2.0 \pm 0.5 \text{ cm d}^{-1}$ , respectively. Assuming a minimum seepage zone width of 3 m (defined as the intertidal zone for a 1 m tide and 20° beach slope), a shoreline length of 20 km (lagoon facing), and an average groundwater  $^{239,240}\text{Pu}$  of  $800 \text{ mBq m}^{-3}$ , the SGD-derived flux of  $^{239,240}\text{Pu}$  to the Bikini lagoon is  $1.6 \times 10^3 \text{ Bq d}^{-1}$ . This is over five orders of magnitude lower than the total Pu input to the lagoon, therefore, the SGD pathway does not appear to be an important source of Pu to surface waters at Bikini (Fig. 7). Using the same approach (groundwater  $^{137}\text{Cs}$  average =  $450 \text{ Bq m}^{-3}$ ), we estimate an SGD-derived  $^{137}\text{Cs}$  flux of  $8.9 \times 10^5 \text{ Bq d}^{-1}$  for Bikini, about three orders of magnitude lower than the total lagoon input flux. Even if we relaxed our assumption of seepage area being limited to the intertidal zone, and scaled the shore-perpendicular groundwater-surface water exchange zone by a factor of 10 (30 m), these SGD radionuclide fluxes would not come close to explaining the lagoon input fluxes.

At Enewetak, we assume the same seepage face (3 m) but estimate the shoreline length at 32 km and a measured groundwater  $^{239,240}\text{Pu}$  of  $1100 \text{ mBq m}^{-3}$ . This yields a SGD  $^{239,240}\text{Pu}$  flux of  $2.1 \times 10^3 \text{ Bq d}^{-1}$ , which is six orders of magnitude less than the total input to the lagoon (Fig. 7). Restricting our SGD flux estimate to Runit Island ( $\approx 4 \text{ km}$  shoreline length), where most of our data was concentrated, would reduce this estimate by a factor of four. The SGD  $^{137}\text{Cs}$  flux is  $9.6 \times 10^4 \text{ Bq d}^{-1}$ , which again is a negligible source of this radionuclide to surface waters. At both Bikini and Enewetak, the SGD flux for  $^{137}\text{Cs}$  is a much greater fraction of the total inputs to lagoon waters relative to  $^{239,240}\text{Pu}$  (Fig. 7); this is consistent with the higher solubility of Cs relative to Pu in oxidizing groundwater (Lujanene et al., 2007). Regardless, SGD is not currently a major source of  $^{239,240}\text{Pu}$  or  $^{137}\text{Cs}$  to seawater at either Bikini or Enewetak, and in particular from the dome at Runit.

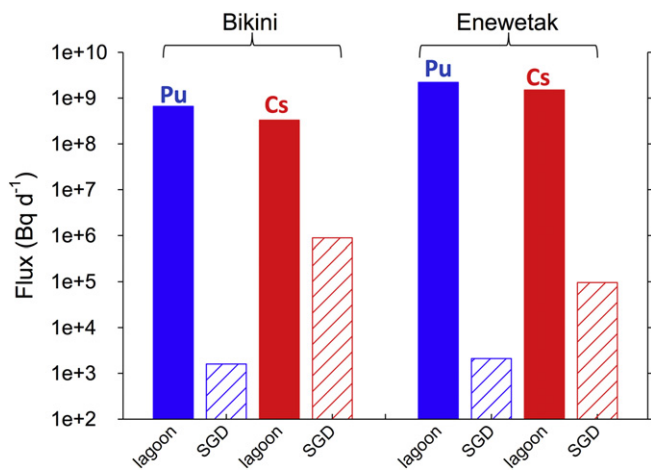


**Fig. 7.** A comparison of the fluxes ( $\text{Bq d}^{-1}$ ) of  $^{239,240}\text{Pu}$  (blue bars) and  $^{137}\text{Cs}$  (red bars) calculated from the lagoon water exchange rates (solid) and derived from radium based SGD calculations (hatched). The rates for Bikini are on left, Enewetak on right. Details in text and data in Table S3.

If the source of Pu and Cs is not SGD, then it must be from exchange from the sediments and associated pore waters. Noshkin and Wong (1979) addressed this issue by assuming that the upper layer of sediments was in equilibrium with the overlying waters, similar to a batch extraction process. Using literature based distribution coefficients ( $K_d = \text{activity on solids/activity in solution}$ ) of  $2.1 \times 10^5$  ( $\text{Bq kg}^{-1}$ ) / ( $\text{Bq L}^{-1}$ ) for  $^{239,240}\text{Pu}$  and average activities in the upper 16 cm of sediment (200 and  $350 \text{ Bq kg}^{-1}$  for Enewetak and Bikini, respectively), they found good agreement with measured Pu levels in the lagoon (their average calculated activities in the lagoon were 800 and  $1500 \text{ mBq m}^{-3}$  in the 1970s for Enewetak and Bikini, respectively). Following the same approach but with our 2015 average lagoon sediment  $^{239,240}\text{Pu}$  activities of  $100 \text{ Bq kg}^{-1}$  (Table 2) we would predict lagoon water activities of  $500 \text{ mBq m}^{-3}$ . For  $^{137}\text{Cs}$ , a similar calculation can be done using a  $K_d$  of 580 (Uchida and Tagami, 2016) and our average sediment activity of  $2 \text{ Bq kg}^{-1}$ , resulting in a predicted lagoon water activity of  $3 \text{ Bq m}^{-3}$ . Both of these are in reasonable agreement with the activities we measured for  $^{239,240}\text{Pu}$  and  $^{137}\text{Cs}$  in the lagoons (Table 2). Thus, to first order, the total supply of radionuclides to the lagoon agrees with a sedimentary source and not the much smaller groundwater fluxes calculated here for the first time using our Ra data and SGD model.

The implications for the Runit dome area are significant. First, we have shown that the exchange of contaminated waters from beneath the dome via SGD is a small source relative to Pu derived from the surrounding seafloor sediments. Yet, Pu isotopes indicate that roughly half of the  $^{239,240}\text{Pu}$  present in the lagoon water is characterized by the low  $^{240}\text{Pu}/^{239}\text{Pu}$  ratios unique to weapons testing carried out on and around Runit Island. Noshkin and Robison (1997) estimate that the sedimentary  $^{239,240}\text{Pu}$  inventories are 44,000 GBq for the entire Enewetak lagoon and only 225 GBq for the top 16 cm of the seafloor sediments in the heavily contaminated area of just under  $1 \text{ km}^2$  offshore Runit Island, though this must be a minimum estimate as we noted that there is  $^{239,240}\text{Pu}$  to at least 2 m at some site near the island (McMurtry et al., 1986). Furthermore, their estimate for the amount of transuranics that were buried under the dome itself is somewhat larger (350 GBq if converted to  $^{239,240}\text{Pu}$  based upon other data from the site), though they noted that their estimates included significant uncertainties. If correct, however, these data suggest that the Pu from this much smaller Runit area (<1%) is more readily available via pore water and sediment exchange processes as a source of Pu to the lagoon ( $\approx 50\%$ ) compared to Pu from other close-in fallout sources. Alternatively, our SGD survey of Runit Island was based on a limited number of groundwater samples (most of them quite shallow) taken at one time point, such that it is

possible we may have missed a Pu plume that would make our island runoff estimates a significant underestimate.

Regardless, without further groundwater and pore water data as well as more detailed study of lagoon sediment radionuclide inventories, we cannot explain or confirm this finding. Additional groundwater surveys should be conducted, as further investigation as to the mobility of Pu from various sources is warranted. It stands to reason that the physical/chemical form of close-in fallout derived from a successful nuclear test will differ from the weapons grade Pu that was dispersed after the dud Quince test. We know for example that Pu derived from the Nevada test site is associated to a higher degree in marine sediments than global fallout Pu (Buesseler and Sholkovitz, 1987; Scott et al., 1983). Likewise Pu from close-in fallout in the Pacific is enriched in deep waters and sediments compared to Pu from global fallout (e.g. Bowen et al., 1980; Buesseler, 1997). With several oxidation states and many different physical/chemical forms, we cannot assume that Pu will behave the same from vastly different sources, which we have seen here even within the Enewetak Lagoon.

## 5. Conclusions

Our overall findings are in agreement with several prior studies regarding the levels and sources of artificial radionuclides at the Bikini and Enewetak Atolls, but also include some important new insights into the magnitude of ongoing sources. Levels of  $^{239,240}\text{Pu}$  and  $^{137}\text{Cs}$  remain elevated, though slightly lower than the 1970's (Fig. 6); more sampling would be needed to reach a more definitive conclusion given the variability within the lagoon and seafloor sediments (Figs. 1 & 2). In particular, Pu is found at orders of magnitude higher activity levels here than elsewhere in the world's ocean and seafloor sediments, whereas Cs is only slightly higher and exceeded today by comparison, in the ocean off Japan near the Fukushima Dai-ichi nuclear power plants.

Using radium isotopes to calculate lagoon water residence times, we estimate an ongoing source of  $^{239,240}\text{Pu}$  and  $^{137}\text{Cs}$  of  $0.7$  to  $2 \times 10^9 \text{ Bq d}^{-1}$  and  $0.3$  to  $1.5 \times 10^9 \text{ Bq d}^{-1}$ , respectively for Bikini and Enewetak (Table S3). While significant, the total flux over the past 60 years is still <0.1% of the amount of  $^{239,240}\text{Pu}$  initially delivered via close-in fallout to the North Pacific and <0.01% for Cs. This explains at why the low  $^{240}\text{Pu}/^{239}\text{Pu}$  ratio water being released from the Enewetak lagoon has not impacted the higher  $^{240}\text{Pu}/^{239}\text{Pu}$  of the North Pacific Ocean, which is characteristic of several high yield thermonuclear tests (Fig. 4). The measured low ratios of  $^{240}\text{Pu}/^{239}\text{Pu}$  in seafloor sediments, the lagoon water and groundwater near Runit Island can be attributed to the 1958 Quince test and possibly other low yield tests in the Runit Dome area (Noshkin and Robison, 1997; Hamilton et al., 2009).

The measurement of radium isotopes in the groundwater near Runit Dome suggest that submarine groundwater discharge from the Runit Dome is not a large source of either Pu or Cs to the lagoon relative to the adjacent seafloor sediments. Thus while the seafloor near Runit Island may account for only a small percentage of the Pu remaining on Enewetak (<1%), it supplies up to half of the Pu found in the lagoon waters. Additional study of the mobility of Pu to explain this will need to take into account the physical and chemical forms of Pu, along with more information on sediment pore water levels and exchange rates. Additional surveys should be conducted beneath the dome to rule out the possibility that groundwater Pu levels are not significantly higher than we observed with our limited dataset.

Importantly, none of the  $^{239,240}\text{Pu}$  or  $^{137}\text{Cs}$  activities in the lagoons or groundwater exceed guidelines for drinking water for the public, though uptake of Pu and Cs through the food chain, exposure to dust and other possible human exposure sources were not evaluated here. Other isotopes of radiological concern include  $^{241}\text{Am}$ , the decay product of  $^{241}\text{Pu}$ , which is found at elevated levels in the seafloor sediments associated with the largest craters at Bikini (Bravo) and Enewetak (Mike). Despite coring in some places almost 1 m deep, we were not able to

sample the entire inventory of these radionuclides, and thus as with prior studies, a complete estimate of the total radionuclide inventory remaining is not possible. We therefore contend that a more comprehensive oceanographic study is needed, similar to those carried out in the 1970's, but including radium isotopes to better characterize current sources. This type of survey will need to be repeated periodically given the large remaining seafloor radionuclide inventories and changing physical and chemical conditions that will accompany sea level rise and deterioration of the Runit Dome.

## Acknowledgements

We could not have conducted this research without assistance from the Captain and crew of the *M/V Alucia* as well as WHOI ship operations for planning and logistical support. Authorization for sampling was provided by the Ministry of Foreign Affairs of the Republic of the Marshall Islands, as well as by Jack Niedenthal and staff at the Bikini Council office for Bikini sampling, and the mayor of Enewetak atoll, Niel Flores as well as Benjamin Maloloy and staff at the Enewetak Council Office for Enewetak sampling. In addition, advice and knowledge based upon the decades of work by Terry Hamilton and colleagues at the Lawrence Livermore National Lab was important for the planning our work, and his staff on Bikini and Enewetak greatly assisted with groundwater sampling. We appreciate the assistance provided during the cruise by John “Chip” Brier and Katlyn Tradd from WHOI, our Marshall Islands observers, Benedict Yamamura, Edward Maddison and Giorgio Note, as well as expedition cinematographer Nathan Tisdale, and volunteer and photographer, Krystyna Wolniakowski. Work on subsampling and analyzing the sediment cores by Ben Duncan and Erin Black is also greatly appreciated. The plutonium analyses of the lagoon and groundwater would not have been possible without the excellent mass spectrometry facilities provided by Steve Peterson and his staff at the Pacific Northwest National Labs. This manuscript was also improved by three anonymous reviewers. Finally, none of this would have been possible without the generous financial support from the Dalio Explore Fund (WHOI #25531513) for the vessel and our post cruise analyses that together resulted in this unique and successful research program. The funding source had no involvement in the project design, interpretation of results or content of this manuscript.

## Appendix A. Supplementary data

Supplementary data to this article can be found online at <https://doi.org/10.1016/j.scitotenv.2017.10.109>.

## References

Aarkrog, A., Dahlgard, H., Holm, E., Hallstadius, L., 1984. Evidence for Bismuth-207 in global fallout. *J. Environ. Radioact.* 1, 107–117.

von Arx, W.S., 1948. The circulation systems of bikini and Rongelap lagoons. *Eos Trans. AGU* 29, 861–870.

Atkinson, M., Smith, S., Stroup, E., 1981. Circulation in Enewetak atoll lagoon. *Limnol. Oceanogr.* 26, 1074–1083.

Bordner, A.S., Crosswell, D.A., Katz, A.O., Shah, J.T., Zhang, C.R., Nikolic-Hughes, I., Hughes, E.W., Ruderman, M.A., 2016. Measurement of background gamma radiation in the northern Marshall Islands. *Proc. Natl. Acad. Sci.* 113, 6833–6838.

Bossew, P., Lettner, H., Hubner, A., 2006. A note on 207 Bi in environmental samples. *J. Environ. Radioact.* 91, 160–166.

Bowen, V.T., Noshkin, V.E., Livingston, H.D., Volchok, H.L., 1980. Fallout radionuclides in the Pacific Ocean: vertical and horizontal distributions, largely from GEOSECS stations. *Earth Planet. Sci. Lett.* 49, 411–434.

Breier, C.F., Pike, S.M., Sebasta, F., Tradd, K., Breier, J.A., Buesseler, K.O., 2016. New applications of KNIcF-PAN resin for broad scale monitoring of radiocesium following the Fukushima Dai-ichi nuclear disaster. *J. Radioanal. Nucl. Chem.* 307, 2193–2200.

Buesseler, K.O., 1997. The isotopic signature of fallout plutonium in the north Pacific. *J. Environ. Radioact.* 36 (1), 69–83.

Buesseler, K.O., Halverson, J.E., 1987. The mass spectrometric determination of fallout  $^{239}\text{Pu}$  and  $^{240}\text{Pu}$  in marine samples. *J. Environ. Radioact.* 5, 425–444.

Buesseler, K.O., Sholkovitz, E.R., 1987. The geochemistry of fallout plutonium in the North Atlantic: II.  $^{240}\text{Pu}/^{239}\text{Pu}$  ratios and their significance. *Geochim. Cosmochim. Acta* 51,

Buesseler, K.O., Aoyama, M., Fukasawa, M., 2011. Impacts of the Fukushima nuclear power plants on marine radioactivity. *Environ. Sci. Technol.* 45, 9931–9935.

Buesseler, K., Dai, M., Aoyama, M., Benitez-Nelson, C., Charrmasson, S., Higley, K., Maderich, V., Masqué, P., Morris, P.J., Oughton, D., Smith, J.N., 2017. Fukushima Daiichi-derived radionuclides in the ocean: transport, fate, and impacts. *Annu. Rev. Mar. Sci.* 9, 173–203.

Burnett, W.C., Aggarwal, P.K., Aureli, A., Bokuniewicz, H., Cable, J.E., Charette, M.A., Kontar, E., Krupa, S., Kulkarni, K.M., Loveless, A., Moore, W.S., Oberdorfer, J.A., Oliveira, J., Ozyurt, N., Povinec, P., Privitera, A.M.G., Rajar, R., Ramessur, R.T., Scholten, J., Stieglitz, T., Taniguchi, M., Turner, J.V., 2006. Quantifying Submarine Groundwater Discharge in the Coastal Zone via Multiple Methods. pp. 498–543.

Burnett, W.C., Peterson, R., Moore, W.S., de Oliveira, J., 2008. Radon and radium isotopes as tracers of submarine groundwater discharge - results from the Ubatuba, Brazil SGD assessment intercomparison. *Estuar. Coast. Shelf Sci.* 76, 501–511.

Charette, M.A., Buesseler, K.O., 2004. Submarine groundwater discharge of nutrients and copper in an urban subestuary of Chesapeake Bay (Elizabeth River). *Limnol. Oceanogr.* 49 (2), 376–385.

Charette, M.A., Buesseler, K.O., Andrews, J.E., 2001. Utility of radium isotopes for evaluating the input and transport of groundwater-derived nitrogen to a cape cod estuary. *Limnol. Oceanogr.* 46 (2), 465–470.

Charette, M.A., Moore, W.S., Burnett, W.C., 2008. Chapter 5 Uranium- and Thorium-Series Nuclides as Tracers of Submarine Groundwater Discharge. pp. 155–191.

Charette, M.A., Breier, C.F., Henderson, P.B., Pike, S.M., Rypina, I.I., Jayne, S.R., Buesseler, K.O., 2013. Radium-based estimates of cesium isotope transport and total direct ocean discharges from the Fukushima nuclear power plant accident. *Biogeosciences* 10, 2159–2167.

Council, N.R., 1982. Evaluation of Enewetak Radioactivity Containment. Final Report. National Research Council.

Dai, M., Buesseler, K., Kelley, J.M., Andrews, J., Pike, S., Wacker, J.F., 2001. Size-fractionated plutonium isotopes in a coastal environment. *J. Environ. Radioact.* 53, 9–25.

Davison, M.L., Hamilton, T.F., Tompson, A.F., 2012. Radioactive waste buried beneath Runit dome on Enewetak Atoll, Marshall Islands. *Int. J. Environ. Pollut.* 49, 161–178.

Diamond, H., Fields, P., Stevens, C., Studier, M., Fried, S., Inghram, M., Hess, D., Pyle, G., Mech, J., Manning, W., 1960. Heavy isotope abundances in Mike thermonuclear device. *Phys. Rev.* 119, 2000–2004.

Froehlich, M., Chan, W., Tims, S., Fallon, S., Fifield, L., 2016. Time-resolved record of  $^{236}\text{U}$  and  $^{239,240}\text{Pu}$  isotopes from a coral growing during the nuclear testing program at Enewetak Atoll (Marshall Islands). *J. Environ. Radioact.* 165, 197–205.

Gerrard, M.B., 2015. America's forgotten nuclear waste dump in the Pacific. *SAIS Review of International Affairs.* 35, pp. 87–97.

Hamilton, T., 2004. Linking legacies of the Cold War to arrival of anthropogenic radionuclides in the oceans through the 20th century. In: Livingston, H.D. (Ed.), *Marine Radioactivity*. Elsevier, pp. 23–78.

Hamilton, T., 2013. A Visual Description of the Concrete Exterior of the Cactus Crater Containment Structure. Lawrence Livermore National Laboratory (LLNL), Livermore, CA.

Hamilton, T.F., Milliès-Lacroix, J.-C., Hong, G.H., 1996.  $^{137}\text{Cs}$  ( $^{90}\text{Sr}$ ) and Pu isotopes in the Pacific Ocean: sources and trends. In: Guegueniat, P., Germain, P., Metivier, H. (Eds.), *Radionuclides in the Oceans: Inputs and Inventories*. EDP Sciences, France, pp. 29–58.

Hamilton, T.F., Martinelli, R.E., Kehl, S.R., McAninch, J.E., 2008. The plutonium isotopic composition of marine biota on Enewetak Atoll: a preliminary assessment. *J. Environ. Monit.* 10, 1134–1138.

Hamilton, T.F., Jernström, J., Martinelli, R.E., Kehl, S.R., Eriksson, M., Williams, R.W., Bielewski, M., Rivers, A.N., Brown, T.A., Tumej, S.J., Betti, M., 2009. *J. Radioanal. Nucl. Chem.* 282, 1019–1026.

Hicks, H., Barr, D., 1984. Nevada Test Site Fallout Atom Ratios:  $^{240}\text{Pu}/^{239}\text{Pu}$  and  $^{241}\text{Pu}/^{239}\text{Pu}$ . Lawrence Livermore National Lab (4pp).

Hirose, K., Aoyama, M., Kim, C., 2007. Plutonium in seawater of the Pacific Ocean. *J. Radioanal. Nucl. Chem.* 274, 635–638.

Hirose, K., Aoyama, M., Povinec, P.P., 2009.  $^{239,240}\text{Pu}/^{137}\text{Cs}$  ratios in the water column of the North Pacific: a proxy of biogeochemical processes. *J. Environ. Radioact.* 100, 258–262.

Hisamatsu, S.I., Sakanoue, M., 1978. Determination of transuranium elements in a so-called “bikini ash” sample and in marine sediment samples collected near Bikini Atoll. *Health Phys.* 35, 301–307.

Kelley, J.M., Bond, L.A., Beasley, T.M., 1999. Global distribution of Pu isotopes and  $^{237}\text{Np}$ . *Sci. Total Environ.* 237/238, 483–500.

Kim, C., Kim, C., Chang, B., Choi, S., Chung, C., Hong, G., Hirose, K., Igarashi, Y., 2004. Plutonium isotopes in seas around the Korean peninsula. *Sci. Total Environ.* 318, 197–209.

Krey, P.W., Hardy, E.P., Pachucky, C., Rourke, F., Coluzza, J., Benson, W.K., 1976. Mass Isotopic Composition of Global Fall-out Plutonium in Soil, Transuranium Nuclides in the Environment, IAEA-SM-199/39. International Atomic Energy Agency, Vienna, Switzerland, pp. 671–678.

Lachner, J., Christl, M., Bisinger, T., Michel, R., Synal, H.-A., 2010. Isotopic signature of plutonium at Bikini atoll. *Appl. Radiat. Isot.* 68, 979–983.

Lindahl, P., Lee, S.-H., Worsfold, P., Keith-Roach, M., 2010. Plutonium isotopes as tracers for ocean processes: a review. *Mar. Environ. Res.* 69, 73–84.

Lindahl, P., Asami, R., Iryu, Y., Worsfold, P., Keith-Roach, M., Choi, M.-S., 2011. Sources of plutonium to the tropical Northwest Pacific Ocean (1943–1999) identified using a natural coral archive. *Geochim. Cosmochim. Acta* 75, 1346–1356.

Livingston, H.D., Povinec, P.P., 2000. Anthropogenic marine radioactivity. *Ocean Coast. Manag.* 43, 689–712.

Lujanienė, G., Motiejunas, S., Sapolaite, J., 2007. Sorption of Cs, Pu and Am on clay minerals. *Journal of Radioanalytical and Nuclear Chemistry.* Vol. 274:pp. 345–353. <https://doi.org/10.1007/s10967-007-1121-1>.

- McMurtry, G.M., Schneider, R.C., Colin, P.L., Buddemeier, R.W., Suchanek, T.H., 1986. Vertical distribution of fallout radionuclides in Enewetak lagoon sediments: effects of burial and bioturbation on the radionuclide inventory. *Bull. Mar. Sci.* 38, 35–55.
- Moore, W.S., 1999. The subterranean estuary: a reaction zone of ground water and sea water. *Mar. Chem.* 65, 111–125.
- Moore, W.S., 2000. Ages of continental shelf waters determined from  $^{223}\text{Ra}$  and  $^{224}\text{Ra}$ . *J. Geophys. Res.* 105, 22,117–123,894.
- Moore, W.S., 2003. Sources and fluxes of submarine groundwater discharge delineated by radium isotopes. *Biogeochemistry* 66, 75–93.
- Moore, W.S., Arnold, R., 1996. Measurement of  $^{223}\text{Ra}$  and  $^{224}\text{Ra}$  in coastal waters using a delayed coincidence counter. *J. Geophys. Res.* 101, 1321–1329.
- Moore, W.S., Reid, D.F., 1973. Extraction of radium from natural waters using manganese-impregnated acrylic fibers. *J. Geophys. Res.* 90, 6983–6994.
- Noshkin, V.E., Robison, W.L., 1997. Assessment of a radioactive waste disposal site at Enewetak Atoll. *Health Phys.* 73, 234–247.
- Noshkin, V., Wong, K., 1979. Plutonium mobilization from sedimentary sources to solution in the marine environment. 3rd Nuclear Energy Agency Seminar on Marine Radioecology, Oct. 1. California Univ., Livermore (USA). Lawrence Livermore Lab, Tokyo, Japan.
- Noshkin, V., Wong, K., Eagle, R., Gatrousis, C., 1975. Transuranics and other radionuclides in Bikini Lagoon: concentration data retrieved from aged coral sections. *Limnol. Oceanogr.* 20, 729–742.
- Noshkin, V.E., Eagle, R.J., Brunk, J.L., Robison, W.L., 1997a. Sediment Studies at Bikini Atoll Part 3. Inventories of Some Long Lived Gamma Emitting Radionuclides Associated with Lagoon Surface Sediments. Lawrence Livermore National Laboratory, Livermore, CA.
- Noshkin, V.E., Eagle, R.J., Wong, K.M., Robison, W.L., 1997b. Sediment Studies in Bikini Atoll Part 2. Inventories of Transuranium Elements in Surface Sediments. Lawrence Livermore National Laboratory, University of California, Livermore, California, p. 94551.
- Noshkin, V., Robison, W., Brunk, J., Jokela, T., 2001. An evaluation of activated bismuth isotopes in environmental samples from the former western Pacific proving grounds. *J. Radioanal. Nucl. Chem.* 248, 741–750.
- Pike, S.M., Dulaiova, H., Buesseler, K.O., 2009. Assessment of size-fractionated species of curium-244 via alpha spectrometry in groundwater. *J. Radioanal. Nucl. Chem.* 282, 1009.
- Pike, S., Buesseler, K., Breier, C., Dulaiova, H., Stastna, K., Sebesta, F., 2013. Extraction of cesium in seawater off Japan using AMP-PAN resin and quantification via gamma spectroscopy and inductively coupled mass spectrometry. *J. Radioanal. Nucl. Chem.* 296, 369–374.
- Pittauer, D., Tims, S.G., Froehlich, M.B., Fifield, L.K., Wallner, A., McNeil, S.D., Fischer, H.W., 2017. Continuous transport of Pacific-derived anthropogenic radionuclides towards the Indian Ocean. *Sci Rep* 7.
- Presley, T.K., 2005. Effects of the 1998 drought on the freshwater lens in the Laura Area, Majuro Atoll, Republic of the Marshall Islands. Scientific Investigations Report, p. 50.
- Robison, W.L., Noshkin, V.E., 1999. Radionuclide characterization and associated dose from long-lived radionuclides in close-in fallout delivered to the marine environment at Bikini and Enewetak Atolls. *Sci. Total Environ.* 237, 311–327.
- Robison, W.L., Conrado, C.L., Bogen, K.T., Stoker, A.C., 2003. The effective and environmental half-life of  $^{137}\text{Cs}$  at Coral Islands at the former US nuclear test site. *J. Environ. Radioact.* 69 (3), 207–223.
- Santos, I.R., Burnett, W.C., Dittmar, T., Suryaputra, I.G.N.A., Chanton, J., 2009. Tidal pumping drives nutrient and dissolved organic matter dynamics in a Gulf of Mexico subterranean estuary. *Geochim. Cosmochim. Acta* 73, 1325–1339.
- Scott, M.R., Salter, P.F., Halverson, J.E., 1983. Transport and deposition of plutonium in the ocean: evidence from Gulf of Mexico sediments. *Earth Planet. Sci. Lett.* 63, 202–222.
- Sebesta, F., 1997. Composite sorbents of inorganic ion-exchangers and polyacrylonitrile binding matrix-I. Methods of modification of properties of inorganic ion-exchangers for application in column packed beds. *J. Radioanal. Nucl. Chem.* 1, 77–88.
- Steinhauser, G., 2014. Fukushima's forgotten radionuclides: a review of the understudied radioactive emissions. *Environ. Sci. Technol.* 48, 4649–4663.
- Uchida, S., Tagami, K., 2016. Comparison of coastal area sediment-seawater distribution coefficients (Kd) of stable and radioactive Sr and Cs. *Appl. Geochem.* 85, 148–153.
- Wu, J., Zheng, J., Dai, M., Huh, C.-A., Chen, W., Tagami, K., Uchida, S., 2014. Isotopic composition and distribution of plutonium in northern South China Sea sediments revealed continuous release and transport of Pu from the Marshall Islands. *Environ. Sci. Technol.* 48, 3136–3144.
- Zheng, J., Tagami, K., Uchida, S., 2013. Release of plutonium isotopes into the environment from the Fukushima Daiichi nuclear power plant accident: what is known and what needs to be known. *Environ. Sci. Technol.* 47, 9584–9595.